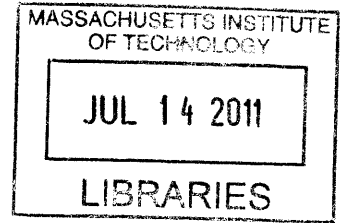A Modeling Framework and Toolset for Simulation and Characterization of the
Cochlea within the Auditory System

by

Samiya Ashraf Alkhairy

S.B. Biological Engineering
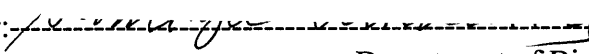Massachusetts Institute of Technology, 2010

SUBMITTED TO THE DEPARTMENT OF BIOLOGICAL ENGINEERING IN
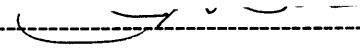PARTIAL FULFILLMENT OF THE REQUIREMENTS FOR THE DEGREE OF

MASTER OF ENGINEERING IN BIOMEDICAL ENGINEERING
AT THE
MASSACHUSETTS INSTITUTE OF TECHNOLOGY
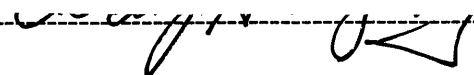
ARCHIVES

JUNE 2011

Signature of Author:
Department of Biological Engineering
May 4, 2011

Certified by:
Christopher Shera
Associate Professor of Otology & Laryngology and Health Sciences & Technology
Thesis Supervisor

Certified by:
Alan Grodzinsky
Professor of Biological, Electrical and Mechanical Engineering

Accepted by:
Forest White
Associate Professor of Biological Engineering
Chairman, Committee for Graduate Students

A Modeling Framework and Toolset for Simulation and Characterization of the Cochlea within the Auditory System

Samiya Ashraf Alkhairy

Submitted to the Department of Biological Engineering on May 15, 2011 in Partial Fulfillment of the Requirements for the Degree of Master of Engineering in Biomedical Engineering

Abstract

Purpose This research develops a modeling approach and an implementation toolset to simulate reticular lamina displacement in response to excitation at the ear canal and to characterize the cochlear system in the frequency domain.

Scope The study develops existing physical models covering the outer, middle, and inner ears. The range of models are passive linear, active linear, and active nonlinear. These models are formulated as differential algebraic equations, and solved for impulse and tone excitations to determine responses. The solutions are mapped into tuning characteristics as a function of position within the cochlear partition.

Objectives The central objective of simulation is to determine the characteristic frequency (CF)-space map, equivalent rectangular bandwidth (ERB), and sharpness of tuning (QERB) of the cochlea. The focus of this research is on getting accurate characteristics, with high time and space resolution. The study compares the simulation results to empirical measurements and to predictions of a model that utilizes filter theory and coherent reflection theory.

Method We develop lumped and distributed physical models based on mechanical, acoustic, and electrical phenomena. The models are structured in the form of differential-algebraic equations (DAE), discretized in the space domain. This is in contrast to existing methods that solve a set of algebraic equations discretized in both space and time. The DAEs are solved using numerical differentiation formulas (NDFs) to compute the displacement of the reticular lamina and intermediate variables such as displacement of stapes in response to impulse and tone excitations at the ear canal. The inputs and outputs of the cochlear partition are utilized in determining its resonances and tuning characteristics. Transfer functions of the cochlear system with impulse excitation are calculated for passive and active linear models to determine resonance and tuning of the cochlear partition. Output characteristics are utilized for linear systems with tone excitation and for nonlinear models with stimuli of various amplitudes.

Stability of the system is determined using generalized eigenvalues and the individual subsystems are stabilized based on their poles and zeros.

Results The passive system has CF map ranging from 20 kHz at the base to 10 Hz at the apex of the cochlear partition, and has the strongest resonant frequency corresponding to that of the middle ear. The ERB is on the order of the CF, and the QERB is on the order of 1. The group delay decreases with CF which is in contradiction with findings from Stimulus Frequency Otoacoustic Emissions (SFOAE) experiments. The tuning characteristics of the middle ear correspond well to experimental observations. The stability of the system varies greatly with the choice of parameters, and number of space sections used for both the passive and active implementations.

Implication Estimates of cochlear partition tuning based on solution of differential algebraic equations have better time and space resolution compared to existing methods that solve discretized set of equations. Domination of the resonance frequency of the reticular lamina by that of the middle ear rather than the resonant frequency of the cochlea at that position for the passive model is in contradiction with Bekesys measurements on human cadavers.

Conclusion The methodology used in the thesis demonstrate the benefits of developing models and formulating the problem as differential-algebraic equations and solving it using the NDFs. Such an approach facilitates computation of responses and transfer functions simultaneously, studying stability of the system, and has good accuracy (controlled directly by error tolerance) and resolution.

Thesis Supervisor: Christopher Shera
Title: Associate Professor of Otology & Laryngology and Health Sciences & Technology

Contents

List of Tables

List of Figures

1 Introduction

Hearing is one of the five major senses in human beings. The auditory system perceives acoustic vibrations in the air in the range of 20 to 20 kHz, transmitted through the ear canal to the ear drum (outer ear) and then through a series of tiny bones (middle ear) to hair fibers in the cochlea (inner ear). The movement of these hair fibers causes electrical nerve firings to be processed eventually by the brain.

Study of the auditory system, which is responsible for processing sensory information, is not only interesting scientifically because of the interconnection between acoustic, mechanical, and electrical systems, but also because of clinical purposes.

As hearing is a major human sense, deafness or hard of hearing is a significant handicap that is high on the priority of health and medicine due to its effect on social and professional interaction. Deafness is a condition in which the ability to sense certain frequencies are completely or partially impaired. This can be due to tearing of the ear drum, damage to the bones, or problems with the cochlea.

This thesis develops a methodology for auditory physical and system modeling and a toolkit for numerical simulation of the outer, middle, and inner ear along with their interactions. Our objective is to form a tool to simulate transmission line models of the cochlea in the time domain. We study its validity as applied to one particular model [22] by performing time domain and frequency analyses.

The toolset can also be used to validate various physiological hypotheses regarding nonlinearity in the active cochlea (eg. origin(s), asymmetry of function) as well as the potential contribution of each of the hypothesized cochlear amplifier (different ways the outer hair cells OHCs produce forces) on the sharpness of tuning of cochlear filters. Such a system allows researchers to study the characteristics of the inner ear especially, and examine the nature of otoacoustic emissions.

1.1 Background

This section provides a background on the auditory system. The anatomy and physiology of the outer, middle, and inner ears are briefly presented here as prerequisite material for the literature survey, and subsequent discussion of the scope of the thesis. In addition, the phenomenon of otoacoustic emissions is outlined as it provides a major opportunity to examine the auditory system.

1.1.1 Auditory System Anatomy

The auditory system is composed of the outer, middle, and inner ears - as illustrated in Figure 1 (adapted from [30]). The outer ear consists of the pinna, ear canal 25-35 mm long starting with concha (opening), and the tympanic membrane (ear drum). The middle ear consists of three bony ossicles (malleus,

incus and stapes) and air cavities opening into pharyngotympanic tube, oval window at the stapes footplate, and the round window. The inner ear consists of the labyrinth, which is part of the vestibular system responsible for maintaining the body's balance, and the cochlea, which plays an important role in the mechanical transmission and neuronal transduction of auditory stimuli [9].
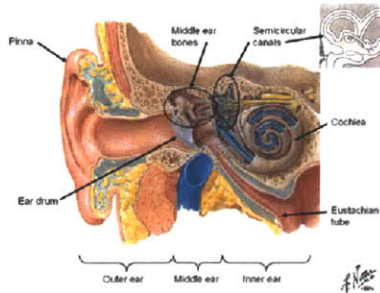
Figure 1: Ear Compartments

The cochlea is a snail-like tube with approximately 2.75 turns. The end with the oval and round windows is the 'base' and the other end is the apex. The tube consists of three channels (scala vestibuli, scala tympani, scala media)for most of its length, as illustrated in Figure 2 (adapted from [30]).

A cross section of the cochlea is shown in Figure 3 (adapted from [6]). The outer channels, the scala vestibuli and scala tympani, are filled with an incompressible fluid called perilymph, and the inner channel, the scala media, is filled with a fluid known as endolymph. At the base, the scala vestibuli opens into the middle ear through the oval window and the scala tympani is connected to the middle ear via the round window. At the apex of the cochlea, the fluid of the scala vestibuli and the scala tympani are continuous. There is a small hole at the apex known as the helicotrema through which the perilymph fluid can flow.

The three channels are separated by Reissner's membrane and the basilar membrane. Reissner's membrane separates the scala vestibuli from the scala media, and is flexible and distortable. Therefore, the Reissner's membrane is generally not included in mechanical, fluid flow, and acoustic models. The basilar membrane is much less distortable in comparison, and is thought to contribute greatly to the tuning along the cochlea [9].

Upon the basilar membrane (BM), sits the organ of corti which consists primarily of the rods of corti, the outer hair cells, and the inner hair cells which convert the signal into neuronal signals that are then transmitted to the auditory faculty in the brain. This is illustrated in Figure 4. The corti contains four rows of hair cells, above which is the tectoral membrane. There are around 16,000 - 20,000 hair cells distributed along the basilar membrane. Each hair cell has about 100 tiny stereocilia of different heights aligned in the order of height on its apical surface, which are leaning on each other in a canonical bundle in the absense of sound waves. This is pictured in Figure 5 (adapted from [6]).
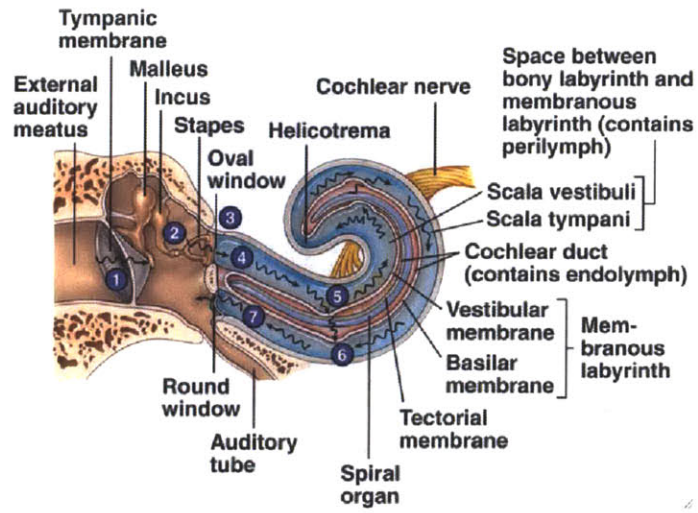
Figure 2: Cochlea
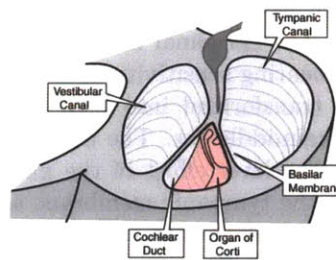
Figure 3: Cochlea Cross Section
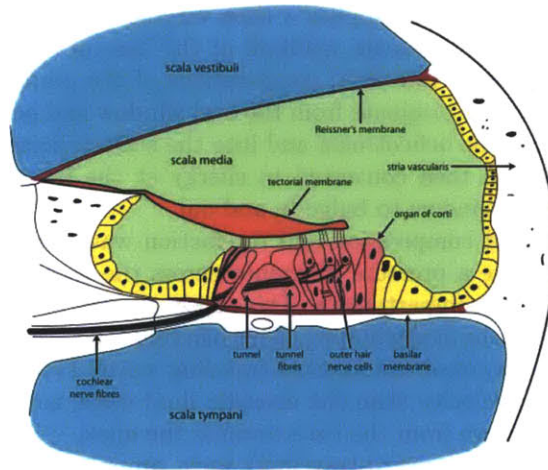
Figure 4: Organ of Corti
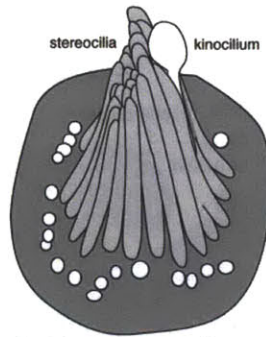
Figure 5: Stereocilia

1.1.2 Auditory System Physiology

An acoustic signal is focused into the concha by the pinna, and transmitted through the ear canal. The ear canal has a resonant frequency of 4 kHz, and the outer ear amplifies hearing sensitivity by a factor of 2 or 3.

The signal is then transformed into bone vibrations as it is transmitted through the bones in the middle ear. The middle ear amplifies the sound thirteen times by utilizing the lever effect of the malleus and incus, and also the area difference between the tympanic membrane and the stapes footplate. The lever is adjustable under muscle action and may actually attenuate loud sounds greater than approximately 75 dB for protection of the ear. As the impedance of the air route is much higher than that of the ossicles, sound is generally assumed to travel only through the ossicles and the air cavities are ignored [8].

The foot of the stapes applies a time-varying pressure to the oval window that is connected to the scala vestibuli at the base of the cochlea. The signal is therefore converted into fluid compressions of the perilymph. The acoustic perilymph vibrations originate from the oval window and pass through the scala vestibuli, around the helicotrema and into the scala tympani. These fluid compression waves are then converted to energy at the base of the cochlea that causes the round window to bulge in and out.

When the fluid compression and rarefaction waves travel through the perilymph, they cause a pressure difference across the cochlear partition between the two perilymph compartments. This causes the BM to bend near the base of the cochlea (near the oval window). This bending is propagated along the length of the BM, and is called the forward-traveling wave. This bending wave propagates at a lower velocity than the acoustic fluid wave, and decreases further in velocity as you move from the base towards the apex.

As the bending (forward-traveling) wave propagates from the base of the basilar membrane (near the stapes and oval window) to the apex (near the helicotrema), its amplitude (vertical displacement of the basilar membrane section)

10

is nonlinearly amplified as the cochlea is an active organ. Depending on the frequency of the sound heard, the vertical displacement of the cochlear partition reaches maximum amplitude at a particular section along the membrane length that resonates with that frequency. If a resonance element at a particular point along the BM is forced at its resonance frequency, the displacement of BM reaches maximum amplitude at that point, after which most of the energy (encoded in the wave amplitudes) is dissipated [9].

Vertical displacement of the cochlear partition causes bending of the hair bundles on the hair cells towards (upwards displacement of the cochlear partition) or away (downwards displacement of the cochlear partition) from the direction of the kinocilium. This bending is associated with a change in influx of positive ions which eventually leads - in inner hair cells, to suppression or enhancement of neurotransmitter release. In particular, stimulation of hair cells which lie on top of the basilar membrane, occurs as a result of shearing motion on the stereocilia of the hair cells. The shear is thought to be caused by the tectorial membrane in the case of the outer hair cells and the endolymph volume velocity in the case of the inner hair cells [13].

The information is then converted to an electric current by opening of a mechanically gated channel on the stereocilia and influx of cations. This process is called mechano(electro)transduction (MET). The upwards displacement of the cochlear partition is associated with an increase in the open probability of the MET receptor channel causes an effective increase in conductance (of mainly potassium); and - driven by the voltage at the apical end of the HC causes an increase in receptor current [2]. The K^+ current influx depolarizes the basolateral membrane of the hair cell and in the OHCs. The depolarization induces a conformational change in a transmembrane motor, thought to be the protein prestin [38, 52], in a manner that decreases the length of the OHC.

This OHC contraction feeds back onto the the displacement of bm and rl. The depolarization of the basolateral membrane also increases the open probability of Ca voltage gated channels. This corresponds to an increase in inwards Ca current, which imposes a low pass filter and results in electrical tuning of voltage. The Ca influx causes neurotransmitter release at the inner hair cell - auditory nerve fiber (IHC-ANF) synapse [18].

The tuning along the cochlea can be described by multiple cochlear filters, each centered around a different characteristic frequency and with a different bandwidth. Tuning is studied physiologically in experimental animals by measuring potentials at the ANF, or using velocimeters. It has also been studied in passive cochlea (where the amplifier is not functional) in human cadavers [50].

As experimental studies on tuning of active cochlea cannot be performed in humans, tuning has also been studied psychophysically in both humans and animals, in an attempt to understand if there is any difference in tuning between humans and animals. Tonotopic maps can be made to illustrate that the maximum amplitude of the forward-traveling wave occurs closer to the base for higher frequencies and closer to the apex for lower frequencies. However, the elements of resonance (in addition to the contribution of the basilar membrane) and cause for resonance are still under study, ie. acoustic fluid wave or forward

traveling BM waves - though many studies suggest that the outer hair cells are the resonating element, and the cause is the fluid compression wave [9].

In summary then, the sound waves travel through the outer and middle ear and finally to the cochlea of the inner ear. In the cochlea the wave propagates along the length of the basilar membrane. The resulting current is then converted into a voltage across the hair cell membrane, and in the case of the inner hair cells, the voltage causes an influx of Ca and therefore release of neurotransmitter to the auditory nerve fiber which is then converted into electrical activity to the central nervous system.

1.1.3   Otoacoustic Emissions

Otoacoustic emissions (OAEs) are low intensity sounds that can be measured at the outer ear and are thought to be 'generated' from the cochlea, usually in response to an input stimulus. These emissions arise because the fluid compression wave or the forward traveling wave is reflected back towards the oval window, through the middle ear and out the ear canal. OAE measurement is a sensitive method for recording cochlear mechanical activity, and is therefore used by clinicians to screen for inner and middle ear transmission pathologies in newborns [24]. If the ear is simulated with a tonal sound (single frequency) the ear emits the same frequency with a phase delay and a lower amplitude. The output signal in response to a tone is known as stimulus frequency otoacoustic emissions - SFOAE.

Several hypotheses have been put forward to explain the mechanism of SFOAE generation, one of which is the coherent reflection theory which suggests that the SFOAEs originate at the point along the cochlea where the input frequency is maximally amplified [44]. Imposing micromechanical irregularities by imposing a 5% jitter on the parameters would allow for the simulation of stimulus frequency otoacoustic emissions (SFOAEs) using this tool, as energy is propagated in both the forward and reverse directions. Studies have used the coherent reflection theory along with a filter model theory to derive the sharpness of tuning from SFOAE experimental data using an approximate relationship between the group delay of the SFOAEs and the group delay of the cochlear traveling wave, and assuming a relationship between the group delay of the cochlear traveling wave and sharpness of tuning. This tool can be used to study the relationship between sharpness of tuning and group delay of cochlear filters based on physical models.

1.2   Literature Survey

Following the broad background outline provided above, this section conducts a literature survey in the major areas related to the thesis. These encompass issues of mechanically tuned elements, behavior of the basilar membrane, mechanoelectric transduction, cochlear amplifier and nonlinearity, and estimation of tuning sharpness of cochlear filters.

1.2.1 Mechanically Tuned Elements

Several hypotheses have been made regarding the nature of the resonating element. The postulates suggest a variety of inner ear components as being a possible resonance element, including the bundles of stereocilia on outer hair cells, the rods of corti, and the basilar membrane.

The first such hypothesis was probably by Helmholtz, who suggested that the resonating elements were the rods of corti that have different stiffnesses and tensions across the length of the BM. However, the fact that these rods are not present in birds and amphibians suggested the possibility of an alternative resonance element. This coupled with the fact that the basilar membrane broadens from base to apex, caused a second theory to arise - one that attributes the resonance to the fibers of the BM.

A third theory, by Bekesy, furthers the second theory by suggesting that the BM is like a gelatinous sheet; and the graded differences in width and stiffness of the basilar membrane are responsible for the differences in the locus of maximal displacement by the traveling waves. A fourth theory, that arose after Beksey's, suggests that resonance is a result of the gradient of stiffness of the bundles in outer hair cell stereocilia, which are shortest at the base and tallest at the apex, as would be expected from such a resonating body [50].

The physiological model used in this study [22] takes into account the mechanical tuning determined by the impedance load of both the BM and the OHCs and hence allows for a graded mechanical-parametric distribution. The height of the hair bundles seems to be mostly taken into account by the mass in the impedance load of the OHC.

Whereas the model used does not take into account motion of the tectorial membrane, recent studies have shown that the tectorial membrane can also carry traveling waves [10] and some studies incorporate the tuning characteristics of the tectorial membrane as part of their models.

1.2.2 Behavior of the Basilar Membrane

Previous data-driven models approximated the behavior of the basilar membrane using a composite elastic model [25]. It used a series of springs in three levels, each with its own stiffness, to model the displacement of the basilar membrane at some location along the cochlea in response to force (mimicking the pressure gradient across the BM). The three levels corresponded well to the histological organization (eg. transverse filaments, and ground substance) of the basilar membrane.

More recent studies have shown a nonlinear relationship between force and displacement of the BM. This is taken into account by the model [21, 22] used in this study. The model collapses the BM and looks at it in only the longitudinal direction (from base to apex), and ignores variability in its mechanical properties along the horizontal/transverse (between the cochlear walls) and vertical (depth) axes. Other models have taken this into account; and modeled the BM behavior as linear and nonlinear orthotropic plates [20]; or modeled the

13

transverse filaments as structures reinforcing the gelatinous base substance of the BM [27].

1.2.3 Mechanoelectrictransduction

Models have previously attempted to relate the motion of the cochlear partition, to the shearing of the OHC's hair bundle and relate that to the change in conductance of the echanoelectrictransduction (MET) channel. Though two major models (gated-spring model and lateral tension model) have attempted to relate the open probability of channels to shearing [47], not many models (we find) attempted to study the relationship between the motion of the cochlear partition and the shear of the hair bundles of the hair cells.

Physical models have shown that the open probability is a function of both velocity and displacement of the cochlear partition [12]. The model used to validate this toolset uses this simplification to relate receptor current to motion of the cochlear partition without modeling the underlying physiological process. Studies have shown that the hair bundle deflection is a nonlinear function of deflection angle, and this is also incorporated only as a mathematical function in the model used in this study.

However, recent studies have shown that as OHCs contract and squeeze the organ of corti, fluid within the organ of corti flows in the spaces, imposing another dimension of complexity [17, 12].

1.2.4 Cochlear Amplifier and Nonlinearity

Two mechanisms have been debated as the primary sources of signal amplification in the cochlea: hair bundle motility and somatic motility (electromotility).

Somatic motility has been shown to occur in vitro in mammals which have much greater amplification than reptiles. However, the major criticism of somatic motility being the major player in cochlear amplification is that the RC time constant of the OHC membrane would impose a low frequency filter that could possibly have a cutoff frequency that would disallow somatic motility from amplifying the characteristic frequencies of the basal sections of the cochlea [36, 38]. However, arguments have suggested that the overall system behavior is not affected by the cutoff frequency of a single component.

In the model we use for this toolset, somatic electromotility is assumed to be the sole cochlear amplifier and this appears to be the case when simulated. Experimental studies have found that in somatic motility, the contraction of the OHC (due to changes in the shape of the transmembrane protein, prestin) is a nonlinear function of basolateral voltage. However, in the model used [22], the only source of nonlinearity is assumed to be mechanoelectrotransduction.

1.2.5 Estimating Tuning Sharpness of Cochlear Filters

One method of expressing the tuning of the cochlear filters, is by using the inverse of the bandwidth (BW). Nondimensionalization by multiplication with characteristic frequency (CF), gives rise to the sharpness of tuning, $Q = CF/BW$ [43].

In the psychophysical literature, characteristic frequency (CF) is the frequency at which the response peaks. Equivalent rectangular bandwidth (ERB) is the bandwidth of the rectangular filter with the same peak response that passes the same total power when driven by white noise. Tuning is measured by QERB, as the ratio of CF to ERB. The QERB can be used to supply parameters used to fit filter models, such as the rounded exponential filter model, in order to generate the tuning curves for various CF along the cochlea.

The tuning curve of the human cochlea cannot be obtained using auditory nerve fiber (ANF) data, unlike animals. Hence, the major approach to estimating the cochlear tuning curves has been to use psychophysical masking methods, which generally uses the power spectrum assumptions suggested by Fletcher [3]. The psychophysical methods make several assumptions, some of which are known to be invalid - such as the linearity of the cochlear amplifier.

However, the psycho-behavioral methods are generally conducted using low signal levels, to be in the linear range of the cochlea. It is also assumed that there is no significant filtering beyond the cochlea, and therefore the filters estimated using the psychophysical methods are reflective of the external ear, middle ear and cochlear filtering as is the case with animal ANF data. Moreover, it is assumed that the majority of the peripheral auditory system filtering is due to the cochlea alone [26].

The psychophysical methods do not all provide the same estimates of tuning sharpness. It is thought that masking phenomenon such as suppression by masker (in the case of simultaneous masking), self suppression (in the case of high signal levels), beats and combination tones (in the case of tone on tone masking), and off-frequency listening (listening using adjacent cochlear filters along the cochlea) affect the estimates of the tuning curves [12]. Certain psycho-behavioral studies have modified their methods to eliminate some of these phenomenon. We use both results for two different types of psychoacoustic studies (which use simultaneous and nonsimulaneous masking) as well as animal ANF data, for comparison with our simulated results of sharpness of tuning.

1.3 Problem Statement

The two top level problems addressed in the thesis are how to simulate the auditory system, and how to compute the characteristics of the cochlea from the simulation. Within the problem set of simulation, issues related to physical modeling, system modeling, and numerical implementation need to be addressed.

Physical modeling is challenging not only because of the complexity of physiology modeled and the variety of subsystems and their interconnections, but also because of the simplifying assumptions that need to be made to be able to represent the model mathematically. Several choices exist in physical modeling, and care has to be taken to use approaches that result in implementable physical models.

An appropriate framework for physical and system modeling is therefore necessary for successful numerical implementation. An approach to system modeling should be taken that allows appropriate study of the properties and

15

numerical simulation. The implementation issues relate to stability, simulation parameters, computational efficiency and sufficient resolution to allow for accurate characterization.

Sufficient effort has to be made to provide solutions to characterization. The characteristics are to be chosen to be consistently computable and relevant to perceptual phenomena. For these purposes, the thesis determines the characteristic frequency (CF)-space map, equivalent rectangular bandwidth (ERB), and sharpness of tuning (QERB) of the cochlea.

1.4 Organization

The problem of developing a modeling framework and toolset for simulation and characterization of the cochlea within the auditory system is best achieved through abstraction into multiple levels. This thesis treats physical model, system model, and numerical implementation as separate layers of abstraction.

The study develops physical models covering the outer, middle, and inner ears. The range of models are passive linear, active linear, and active nonlinear. These models are formulated as algebraic differential equations, and solved for impulse and tone excitations to determine responses. The solutions are mapped into tuning characteristics as a function of position within the cochlear partition.

There are a number of issues addressed in this thesis. These relate to physical modeling, system modeling, and an implementable toolset that simulates the system. Physical modeling is conducted for the outer, middle, and inner ears, even though the focus is on the cochlea. This is because excitation is applied at the ear canal and the cochlea is not isolated from the middle ear.

Particular attention is paid to physical modeling of the cochlea. Acoustic models are used for transmission in the perilymph, and electrical and mechanical models for the cochlear partition and the outer hair cell.

Chapter 2 develops physical models. The objective here is to focus on the mechanical, acoustic, and electrical laws that govern various parts of the auditory system, and to formulate them mathematically. The development is not distracted by issues that govern the entire system or its characterization or numerical issues.

Chapter 3 maps the physical models into a state space formulation. This entails specification of the state variables and space discretization, differential algebraic equations, excitation and response. Issue of stability arise and suitable methods are employed to address these. The chapter ends with development of methods for extracting response and system characteristics from excitation and response.

Chapter 4 provides the toolset for simulation of the auditory system. A particular type of differential algebraic equations solver is proposed, and solver parameters are calculated based on auditory system characteristics known to date.

Chapter 5 applies the toolset to calculate the traveling wave, tuning characteristics, spectra, cochlear map, ERB, QERB, and group delay. These results are validated against available information.

2 Physical Model

This chapter presents the physical equations that model the auditory system. These equations relate the components of the ear and the interfaces between these components [21, 22, 33]. The equations are supplemented with boundary conditions [21, 22, 33] to uniquely determine the solution of the equations.

The components are external canal, diaphragm, ear drum, malleus, incus, stapes, round window, scala vestibuli, scala tympani, reticular lamina, basilar membrane, and ohc. These components, interfaces, and boundaries are listed in Table 1. Boundary conditions are provided at the base and apex of the scala vestibuli, as well as between the basilar membrane and the fluid, and between the ohc and basilar membrane and reticular lamina.

The physical equations govern mechanical, acoustic, and electrical phenomena. Mechanical equations govern the outer and middle ear components comprising of external canal, diaphragm, ear drum, malleus, incus, stapes, round window, basilar membrane, reticular lamina and the contraction of ohc. Acoustic equations govern the fluid motion in the scala vestibuli and scala tympani. Electrical equations characterize the apical current, basolateral voltage and charge displacement in the ohc. Generic notation for the variables and parameters are tabulated in Table 2.

To enhance readability, notation is standardized in Table 3 to indicate time derivative, effect of a source on an object, and differences between variables. The variables are subscripted with element. For example, P_d denotes presssure at the diaphragm.

Table 1: Notation - Components and Interfaces

Notation	Description
ec	External Canal
b	Speaker Base
d	Diaphragm
$b\|d$	Base - Diaphragm Interface
ed	Ear Drum
$d\|ed$	Diaphragm-Ear Drum Interface
m	Malleus
edw	Middle Ear Wall
$edw\|m$	Middle Ear Wall - ED/Malleus Complex Interface
i	Incus
$m\|i$	Malleus-Incus Interface
s	Stapes
$i\|s$	Incus-Stapes Interface (Incudo-stapedial Joint)
w	Round Window
sv	Scala Vestibuli
st	Scala Tympani
rl	Reticular Lamina
$sv\|rl$	Scala Vestibuli Reticular Lamina Interface
bm	Basilar Membrane
ohc	OHC
$bm\|wc$	Basilar Membrane - Cochlear wall interface

Table 2: Notation - Variables and Parameters

Mechanical variables and parameters	
Notation	**Description**
F	Translational Force
x	Translational Displacement (contraction in the case of OHC)
v	Translational Velocity
k	Stiffness
m	Mass
c	Compliance
Acoustic variables and parameters	
Notation	**Description**
P	Acoustic Pressure
U	Volume Velocity
V	Particle Velocity
Electric variables and parameters	
Notation	**Description**
V	Voltage
i	Current
Q	Charge

Table 3: Notation - Miscellaneous

Notation	Description
t	Time
V'	Time derivative of variable V
$_sV_o$	Variable on object o by source s eg. $_{ohc}F_{bm}$ is force on bm by ohc
V^i	Variable at section i of cochlea
P_{st-sv}	$P_{st} - P_{sv}$

2.1 Subsystem Models

This section physically models the subsystems of the auditory organ. A subsystem may be centered around an interface as is frequently the case in outer and middle ear, or a transformation as is often the case in the cochlea.

In all cases, a formulation approach is utilized that makes it amenable to utilization in system model of Chapter 3. Thus for example, physical equations are written in terms of derivatives of velocities rather than double derivatives of displacement. Also, an algebraic equation is written with left hand side equal to zero and the right hand side equal to the algebraic expression. A multiplier of zero is generally added on the left hand side to indicate the row in the system formulation in which the algebraic expression is placed. The physical equations are reformulated in terms of state variables as explained in Chapter 3.

2.1.1 Outer and Middle Ear

The subsystems in the outer and middle ears are speaker base - diaphragm, diaphragm - ear drum, ear drum - malleus, malleus - incus, incus - stapes, stapes and round window - fluid.

Speaker base-diaphragm The stimulus is presented by placing a speaker in the ear canal. The base of the speaker is fixed and points towards the outer part of the ear canal. The diaphragm of the speaker is at its front end pointing towards the ear drum. Excitation in the form of external force, $F(t)$, is applied at the diaphragm, resulting in its vibration. The interface between the base and diaphragm is modeled as a parallel spring and damper with stiffness $k_{b|d}$ and compliance $c_{b|d}$.

Three forces act on the diaphragm with mass m_d to produce displacement x_d and velocity v_d. The external force (excitation) is $F(t)$. The force from the spring and damper is $(-k_{b|d}x_d - c_{b|d}v_d)$, since the base is fixed and hence, $x_b = 0$ and $v_b = 0$. The force acting on the diaphragm from the ear canal between the diaphragm and the ear drum is $-_{d|ed}P_d A_d$. Here A_d is the area of the diaphragm and $d|ed$ is the air between the diaphragm and the ear drum that exerts pressure $_{d|ed}P_d$ on the diaphragm.

The subsystem model is governed by the following equations:

$$x'_d = v_d \tag{1}$$

$$m_d v'_d = F(t) - k_{b|d}x_d - c_{b|d}v_d -_{d|ed} P_d A_d \tag{2}$$

Diaphragm - Ear Drum The air space between the diaphragm and the ear drum is assumed to be acoustically lossless and to be shorter than the smallest wave length of interest (0.05 mm) and hence $_{d|ed}P_d \approx -_{d|ed}P_{ed}$. The pressure on the diaphragm is denoted by $P_d =_{d|ed} P_d$.

The air space between the diaphragm and ear drum (ED) is approximated as an acoustic compliance, so that the pressure is directly proportional to the volume of air in the closed space. This is illustrated by the equation below. It is

assumed that the displacement of the ear drum, x_{ed}, is equal to the displacement of the malleus, x_m, as the malleus is assumed to be rigidly fixed to the ED. The areas of the diaphragm and ear drum are denoted by A_d and A_{ed}.

$$0 * P'_d = P_d - Q_s(A_d x_d - A_{ed} x_m) \tag{3}$$

Malleus-incus The interface that determines the relationship between displacement of the malleus and incus is approximated as lever; the incus is connected to the lever at a lower position than the malleus. As the torques at the two positions are equal, $\frac{x_{li}}{x_{lm}} = \frac{_{lm}f_m}{_i f_{li}} \equiv g_l$. Therefore, $_{lm}f_m = g_{li}f_{li}$.

Middle ear wall - ED The interface between the malleus and ED is assumed to be rigid, and hence approximated as a single body. The mass of the ED is considered insignificant relative to the mass of the malleus.The wall-ED system interface is approximated as a spring-dashpot system in parallel, where the wall position is fixed. The forces on the ED-malleus body (for which we use the subcript m) are therefore $_{d|ed}P_{ed}$ and the forces by the wall-malleus interface, as well as the force by the lever approximating the malleus-incus interface, $_{lm}f_m = -g_{li}f_{li}$. This yields,

$$x'_m = v_m \tag{4}$$

$$m_m v'_m =_{d|ed} P_d A_e d - k_{edw|m} x_m - c_{edw|m} v_m + g_{li}f_{li} \tag{5}$$

Incus-stapes The interface between the incus and the stapes is approximated as a mass-dashpot configuration. The incus is estimated to be massless, with forces $_{li}f_i$ and $_{i|s}f_i = F_k + F_c$ acting on it on opposite sides. The force balance can be therefore written as $0 = k_{i|s}(x_s - x_i) + c_{i|s}(x'_s - x'_i) -_{li} f_i$. Assuming a rigid connection between the lever and the incus and the lever and the malleus, allows for the substitution $x_i = x_{li} = g_l x_m$, which gives,

$$x'_s = v_s \tag{6}$$

$$0 *_i f'_{li} =_i f_{li} - k_{i|s}(x_s - g_l x_m) - c_{i|s}(v_s - g_l v_m) \tag{7}$$

Stapes and round window - fluid The footplate of the stapes is connected to the oval window that transmits the motion into the scala vestibuli at the base of the cochlea. The perilymph of the scala vestibuli is connected through the helicotrema to the perilymph of the scala tympani. The round window is connected to the scala tympani at the base of the cochlea, and opens into the middle ear. In the model in equation 8, The mechanical impedance of the round window on the cochlea is incorporated as part of the stapes - cochlea interface. The forces acting on the stapes with an effective mass of $m_s + m_w$ are the the stapes/round window-cochlea interface as well as the forces by the incus-stapes interface. According to equation, the forces by the incus-stapes interface can be

approximated as $-_i f_{li}$, as the incus is massless. The force by the base of the cochlea $P_{fl}^{base} A_s$ is approximated to act directly on the stapes.

$$(m_s + m_w)v_s' = -_i f_{li} - (k_{s|fl} + k_{w|fl})x_s - (c_{s|fl} + c_{w|fl})v_s - P_{fl}^{base} A_s \qquad (8)$$

2.1.2 Cochlea

Subsystems in the cochlear are stapes - perilymph base, perilymph apex- helicotrema, perilymph - cochlear partition, cochlear partition - HC receptor current, HC receptor current - voltage, ohc charge accumulation - contraction, ohc voltage - contraction force transformation, ohc - cochlear partition feedback.

Stapes - perilymph^{base} The footplate of the stapes is connected to the oval window that links the middle ear to the scala vestibuli of the cochlea. The oval window is assumed to have negligible impedance, and the motion of the stapes is considered directly on the compression and rarefaction of perilymph at the base of the cochlea. According to Newton's second law, this can be approximated as,

$$-\rho * v_s' = \frac{\partial P_{sv}}{\partial x} \qquad (9)$$

P_{sv} is approximated and P_{fl} is used instead, as P_{st} is considered negligible relative to P_{sv} due to power loss as the acoustic wave travels through the perilymph. This results in equation 10. It should be noted that the notation P_{fl}^i is for nodes rather than sections, so the nodes P_{fl}^{base} and P_{fl}^{base+1} surround the basal section.

$$-\rho * v_s' + 0 * P_{fl}^{base} = \frac{P_{fl}^{base+1} - P_{fl}^{base}}{\Delta x} \qquad (10)$$

Wave propagation along the perilymph The propagation of the acoustic wave in the perilymph, is partly described by Newton's second law, which relates the pressure and volume velocity as in equation 11

$$\frac{\partial P_{fl}}{\partial x} = -\frac{\rho}{A_{par}} U_{fl}' \qquad (11)$$

The fact that the cochlear partition is movable, is taken into account in the equation of mass conservation to yield equation 13. The second wave equation is derived from the equation of continuity taking into account the change in volume of the fluid as x_{rl} changes. Thus, accounting for wall vibration

$$-\frac{\partial P}{\partial x} = \rho \frac{\partial (U/A_{par})}{\partial t} \qquad (12)$$

$$-\frac{\partial U}{\partial x} = \frac{1}{\rho c^2} \frac{\partial P A_{par}}{\partial t} + \frac{\partial A_{par}}{\partial t} \qquad (13)$$

$$\frac{\partial U}{\partial x} = w_{par} v_r l \tag{14}$$

Equation 14 implies that volume velocity is dependent on the change in displacement and width of the BM [32, 35].

Equations 11 and 14 are combined to get,

$$0 * P_{fl}^i - \frac{\rho w_{part}^i}{Areas^i} v_{rl}' = \frac{P_{fl}^{i+1} - 2P_{fl}^i + P_{fl}^{i-1}}{(\Delta x)^2}; \tag{15}$$

It should be noted that an assumption is made that the cochlear partition sections are not directly coupled among themselves, but instead coupled only through perilymph.

Perilymph - helicotrema   The boundary condition at the apex is chosen to be inductive and is approximated by an open ended tube, such that,

$$P_{fl}^{apex} = \rho \frac{V}{A^2} \frac{\partial U}{\partial t} \tag{16}$$

In the above equation, V is volume and A is area. This can be rewritten as,

$$P_{fl}^{apex} = m_h \frac{\partial U}{\partial t} \tag{17}$$

where m_h is the effective mass per unit area at the helicotrema. Though the x_{rl} motion at the apex is not clamped, the boundary condition at the apex assumes rigid walls unlike the rest of the cochlea, and hence uses the traditional equation of continuity as part of the wave equation [3]. Taking into account this aspect of the wave equation, $\frac{\partial U}{\partial t} = -\frac{A}{\rho}\frac{\partial P}{\partial x}$, yields,

$$0 * P_{fl}'^{apex} = \frac{\rho}{A^{apex} m_h} * P_{fl}^{apex} + \frac{P_{fl}^{apex} - P_{fl}^{apex-1}}{\Delta x} \tag{18}$$

Perilymph - Cochlear partition   The acoustic impedance of Reissner's membrane is considered negligible and hence the pressure in the scala media is the same as the pressure in the scala vestibuli. Thus, we are only interested in the differential pressure $P_{fl} \equiv P_{sv} - P_{st}$ as the pressure driving the vertical motion of the cochlear partition. Whereas the basilar membrane is considered sturdy, the reticular membrane is simply the tight joining of the OHCs and the phalangeal process of the Deiter's cells [9], and hence considered deformable. Since the impedance is dominated by the BM as opposed to the RL, P_{fl} is approximated to act on the BM.

The forces acting on the BM are therefore P_{fl} and the force by the cochlear wall -BM interface along the entire length of the cochlear acting in the negative direction. This is reflected in equation 19. In the expression below, $m_{bm|wc}, c_{bm|wc}, k_{bm|wc}$ are per unit area, and the equation does not take into account spatial interaction between neighboring sections of the basilar membrane.

$$m_{bm} v_{bm}' = -P_{fl} - c_{bm|wc} v_{bm} - k_{bm|wc} x_{bm} \tag{19}$$

Cochlear partition - receptor current As the cochlear partition moves in response to the stimuli, the stereocilia on each hair cell move towards or away from the kinocilium. These stereocilia carry mechanoelectric transduction (MET) channels whose probability of opening changes with stereocilia displacement. This dependence is thought to be due to the tension in a spring-like component linking the MET gates of one stereocilia to the next stereocilia according to the gating-spring model. Changing the probability of an open gate of the MET channels alters the amount of flow of potassium and other positive ions (driven by the transmembrane voltage of the apical side of the HCs) into the hair cells. This mechanoelectric transduction is modeled by equation 20, where i_{rec} is the receptor current relative to the current at rest.

$$i_{rec} = \alpha_{v_{rl}} v_{rl} + \alpha_{x_{rl}} x_{rl} \tag{20}$$

It should be noted that this mechanoelectric transduction does not occur in the passive system, as the generator for the voltage gradient across the HCs apical membrane (which drives the receptor current) in the stria vascularis is an energy-requiring process that is not functional in cadavers.

The receptor current is thought to be a strongly nonlinear function of cochlear partition displacement, and this is incorporated in the nonlinear implementation of the model by substituting equation 20 with equation 21. The change in transduction current with cochlear partition motion is greatest for small motion amplitudes (in the linear range). Therefore, a tanh function is used to model the nonlinearity. It should be noted that the empirical function has experimentally been found to be asymmetric [9]. This asymmetry is due to the fact that the probability of the MET channels being open at rest is 10%.

$$i_{rec} = \frac{i_{max}}{2} \tanh \frac{2(\alpha_{v_{rl}} v_{rl} + \alpha_{x_{rl}} x_{rl})}{i_{max}} \tag{21}$$

Receptor current - voltage The change in apical current alters the transmembrane voltage of the basalateral side of the HCs. In the HCs, the voltage across the basolateral membrane is responsible for driving the influx of Ca^{++} through calcium voltage-gated channels. Specifically, the (apical) receptor current into the OHC is associated with the transmembrane-voltage-driven flow through basolateral Ca^{++} conductive channels (with conductance G_{ohc}), as well a capacitative current (as the membrane bilayer of the OHC has a conductance C_{ohc}), and the current associated with the time derivative of the charge displacement Q_{ohc}. This is modeled in equation 22, where V_{ohc} is the basolateral transmembrane voltage of the OHC relative to the resting voltage.

$$i_{rec} = C_{ohc} Volt'_{ohc} + G_{ohc} Volt_{ohc} + Q'_{ohc} \tag{22}$$

OHC charge accumulation - contraction The charge accumulation is associated with a change in length of OHC. This process is thought to be mediated by prestin, an OHC transmembrane motor protein, that is hypothesized to

24

change orientation of its charge groups as a function of voltage. The configurational changes in prestin translate into the contraction or extension of the length of OHC. The relationship between charge Q_{ohc} and contraction x_{ohc} is assumed to be linear as seen in equation 23. In the equation below, a peizo-electric model is used to relate the OHC strain to the charge accumulation.

$$x_{ohc} = T_{ohc}Q_{ohc} \tag{23}$$

OHC voltage - contraction force transformation   An impedance is assumed against the contraction and extension of the OHCs [21]. The spring constant is an expression of OHC internal stiffness, and an assumption is made that the connections between the OHC and BM and between the OHC and RL are rigid. This is represented as follows. The driving force is assumed to be generated from the differential voltage (voltage of the OHC membrane - voltage of prestin).

$$f_{ohc} = m_{ohc}v'_{ohc} + c_{ohc}v_{ohc} + k_{ohc}x_{ohc} \tag{24}$$

$$f_{ohc} = \frac{V - \tilde{V}}{T} \tag{25}$$

$$\tilde{V} = Q_{ohc}/Cg \tag{26}$$

OHC - cochlear partition feedback   The change in length of the OHC feeds back onto the motion of the cochlear partition. This feedback is thought to act as a cochlear motor amplifier. Contraction of the OHC, would cause a positive displacement in the BM and a negative displacement in the RL, thereby bringing them closer together. This can be written as equation 27, where x_{ohc} is the contraction, rather than displacement of OHC. This is approximated as,

$$x_{bm} = x_{rl} + x_{ohc} \tag{27}$$

Further simplifying assumptions   The Ca^{++} current further tunes the voltage across basolateral membrane [9]. In this model, tuning is assumed to have a negligible effect on the tuning detected at the auditory nerve fibers (ANF), as experimental studies have shown tuning at the cochlear partition is approximately representative of tuning measured at the ANF [9]. This model also ignores the effects of stapedius and the other muscle of the middle ear and the feedback effects of central nervous system (CNS) descending systems.

Governing equations   The equations governing the cochlear partition are combined to yield the following equations in terms of state variables. The equations governing the P_{fl} state variables are in equations 10, 15 and 18 above.

$$x'_{rl} = v_r l \tag{28}$$

25

$$Q'_{ohc} = \frac{v_{ohc}}{T_{ohc}};\tag{29}$$

$$v'_{ohc} = -\frac{c_{ohc}v_{ohc} + k_{ohc}T_{ohc}Q_{ohc}}{m_{ohc}} + \frac{Volt_{ohc} - Q_{ohc}/Cg_{ohc}}{T_{ohc}m_{ohc}}\tag{30}$$

$$V'_{ohc} = \frac{i_r - G_{ohc}V_{ohc} - v_{ohc}/T_{ohc}}{C_{ohc}}\tag{31}$$

$$v'_{rl} + v'_{ohc} = -\frac{c_{bm|wc}(v_{rl} + v_{ohc}) + k_{bm|wc}(x_{rl} + T_{ohc}Q_{ohc})}{m_{bm}} - \frac{P_{fl}}{m_{bm}};\tag{32}$$

Equations 32 was later rewritten as equation 33 for purposes of stabilization, as explained in section 3.4

$$\begin{aligned}v'_{rl} &= -1 * (-\frac{c_{ohc}v_{ohc} + k_{ohc}T_{ohc}Q_{ohc}}{m_{ohc}} + \frac{Volt_{ohc} - Q_{ohc}/Cg_{ohc}}{T_{ohc}m_{ohc}})\\ &\quad -\frac{c_{bm|wc}(v_{rl} + v_{ohc}) + k_{bm|wc}(x_{rl} + T_{ohc}Q_{ohc})}{m_{bm}} - \frac{P_{fl}}{m_{bm}}\end{aligned}\tag{33}$$

Derivation of cochlea equations, is based on the following equations. From 23, we take the derivative with respect to time to get 29. To get 30, we start with 24,

$$v'_{ohc} = \frac{f_{ohc} - c_{ohc}v_{ohc} - k_{ohc}x_{ohc}}{m_{ohc}}\tag{34}$$

substitute x_{ohc} with 23, and substitute, f_{ohc} with the terms in equations 25 and 26.

To get 33, we start with 27, and take the time derivative so that,

$$v'_{rl} = v'_{bm} - v'_{ohc}\tag{35}$$

We substitute v'_{bm} with 19

$$v'_{rl} = -\frac{P + c_{bm|wc}v_{bm} + k_{bm|wc}x_{bm}}{m} - v'_{ohc}\tag{36}$$

We then resubstitute v_{bm} and x_{bm} based on 27, and then substitute v'_{ohc} using 30 to finally get 33

To get 31, we rearrange 22, to get,

$$V' = \frac{i_r - GV - Q'}{C}\tag{37}$$

substituting Q' using 29, we get 31

26

2.2 Parameter Values

The parameters used for implementation are in Tables 4 and 5. For parameters that vary along the cochlea, the basal, middle and apical parameters are listed in that order. These parameters are used to determine the values for the remaining cochlear sections using log-quadratic interpolation [22] in accordance with equation 39 where $pm_{base}, pm_{mid}, pm_{apex}$ are the parameter values for the apical, middle and basal sections of the cochlea and x_{apex} is the length of the cochlear partition.

$$a = \frac{2}{x_{apex}^2} ln\left(\frac{pm_{mid}^2}{pm_{base}pm_{apex}}\right) \tag{38}$$

$$b = \frac{1}{x_{apex}} ln\left(\frac{pm_{apex}}{pm_{base}}\right)$$

$$pm_i = pm_{base}exp(ax_i(x_{apex} - x_i) + bx_i)$$

We initially (before stabilization) used the parameters in table 4 [22] while using the parameter A_s from table 5 [23] and approximating ρ of perilymph by that of water. However, for the number of space sections we initially ran for validation purposes, even the passive implementation was unstable and hence too stiff to simulate using ode23t with low error tolerances (section 4.1).

We then instead simulated the physical model using the parameters in Table 5. Whereas the passive simulation was stable, the active linear and nonlinear simulations were both unstable, and the active linear implementation was too stiff to simulate for an appropriate number of sections and simulation time.

We switched to using ode15s (stiffer ode solver than ode23t - section 4.1) and allowed for increased error tolerance (see section 4.2). Then we looked into subsystem stabilization and altered the governing equations accordingly (section 3.4). This removed the instability of the active nonlinear version and greatly decreased the instability of the active implementations using the parameters in table 5. The active linear implementation appeared to be marginally unstable for apical sections, but was still unstable (though it blows up much less) for the basal sections.

After modifying the governing equations, we tested for system stability (section 3.5) and found that the system was unstable in the active linear and nonlinear implementations while using the parameters in table 5. Interestingly, the stability of the passive and active implementations of the system while using the parameters in table 4 depended on the number of space sections used for discretization. We therefore finally resolved to use the parameters in table 4 using 700 space sections for which the system stability test and the implementation proved that the passive and active implementations were stable. We then decreased the error tolerances to their original values as in section 4.2.

Table 4: Parameter values - cgs units [22]

Parameter	Value
m_d	5e-3 g
$k_{st\|d}$	4e8 g/s^2
$c_{st\|d}$	1.4e3 g/s
A_d	0.75 cm^2
A_{ed}	0.5 cm^2
g_l	0.7
Q_c	8.5e5 dyn/cm^5
m_m	8.5e-3 g
$k_{edw\|m}$	1.5e5 g/s^2
$c_{edw\|m}$	20 g/s
$k_{i\|s}$	5e6 g/s^2
$c_{i\|s}$	400 g/s
m_s	5e-3 g
m_w	5e-3 g
$k_{s\|fl}$	5e5 g/s^2
$k_{w\|fl}$	1.5e5 g/s^2
$c_{s\|fl}$	80 g/s
$c_{w\|fl}$	20 g/s
T_{ohc}	8.02e2 cm/statC
c_{ohc}	[9.4e-4, 9.2e-4, 2.7e-3] g/s
k_{ohc}	[200, 11, 0.76] g/s^2
m_{ohc}	[2.8e-8, 5e-7, 2.8e-5] g
Cg_{ohc}	[16.2, 29.7, 63] statF
$\alpha_{x_{rl}}$	[5.337e-11, 2.068e-11, 6.67e-12] statA/cm
$\alpha_{v_{rl}}$	[1.468e-13, 6e-14, 2.27e-14] statA/cm
G_{ohc}	[8.1761e4, 4.5822e4, 2.965e4] statSiemens
C_{ohc}	[12.6, 28.8, 71.1] statF
$c_{bm\|wc}$	[1.5, 3.2, 8.6] $g/(s * cm^2)$
$k_{bm\|wc}$	[5.9e5, 4e4, 1.6e3] $g/(s^2 * cm^2)$
m_{bm}	[3.8e-5, 2.8e-4, 2.1e-3] g/cm^2
A_{par}	[6.3e-2,1.4e-2, 3.1e-3] cm^2
w_{par}	[0.031, 0.040, 0.051] cm
ρ	0.98 g/cm^3
m_h	110; g/cm^4
i_{max}	[2.01, 0.96, 0.249] statA

Table 5: Parameter values - cgs units [23]

Parameter	Value
m_d	5e-3 g
$k_{st|d}$	4e8 g/s^2
$c_{st|d}$	1.4e3 g/s
A_d	0.75 cm^2
A_{ed}	0.5 cm^2
g_l	0.7
Q_c	8e5 dyn/cm^5
m_m	8.5e-3 g
$k_{edw|m}$	1.5e5 g/s^2
$c_{edw|m}$	20 g/s
$k_{i|s}$	5e6 g/s^2
$c_{i|s}$	400 g/s
m_s	1e-2 g
m_w	5e-3 g
$k_{s|fl}$	6.5e5 g/s^2
$k_{w|fl}$	1.5e5 g/s^2
$c_{s|fl}$	100 g/s
$c_{w|fl}$	20 g/s
A_s	6.25e-2 cm^2
T_{ohc}	8.02e2 cm/statC
c_{ohc}	[9.39e-4,9.2e-4,0.002] g/s
k_{ohc}	[1.96e+02,10.65,0.764] g/s^2
m_{ohc}	[2.8e-8, 5e-7, 2.8e-5] g
Cg_{ohc}	[1.8e-18,3.3e-18,7.0e-18] statF
$\alpha_{x_{rl}}$	[1.63e-05,6.23e-06,2.04e-06] statA/cm
$\alpha_{v_{rl}}$	[4.36e-8,1.78e-8,6.8e-9] statA/cm
G_{ohc}	[9.1e-15,5.1e-15,3.3e-15] statSiemens
C_{ohc}	[1.4e-18,3.225e-18,7.92e-18] statF
$c_{bm|wc}$	[48.9,79.8,1.7e+2] $g/(s * cm^2)$
$k_{bm|wc}$	[1.9e+07,1.007e+06,3.14+04] $g/(s^2 * cm^2)$
m_{bm}	[0.00124,0.0071,0.041] g/cm^2
A_{par}	[6.25e-2,1.39e-2, 3.1e-3] cm^2
w_{par}	[0.031, 0.040, 0.051] cm
ρ	2 g/cm^3
m_h	110; g/cm^4
i_{max}	[6.667e-10, 3.226e-10, 8.33e-11] statA

3 System Model

This chapter develops a system of equations that are simulated through numerical implementation in the next chapter to compute response of the auditory system to an excitation. A number of alternatives exist for simulation of the physical model equations of Chapter 2. The system model organizes the physical equations of the previous chapter as differential algebraic equations incorporating all of the auditory subsystems.

Section 3.1 presents the state variables of the system. Section 3.2 formulates the dynamics of the state variables as a system of differential algebraic equations. Section 3.3 manipulates the system to ensure subsystem stability. Section 3.4 discusses methods to determine stability of the entire system. Section 3.5 presents the excitations utilized and the responses calculated. Section 3.6 summarizes the method used in computing the frequency response of the cochlea. Section 3.7 presents methods for frequency domain characterization, such as characteristic frequencies.

3.1 State Variables

A system of equations may be developed in the frequency domain to directly provide insight into frequency domain characteristics, or in the time domain to study its dynamics. The frequency domain approach is restrictive to linear time invariant systems. As our physical models incorporate non-linear options, the system is modeled in the time domain rather than the frequency domain, with frequency characteristics obtained from time domain dynamics.

In addition to investigation of the nonlinear phenomena, interest lies in studying multiple responses to an excitation, such as displacement of the stapes and displacement of the reticular lamina throughout its length. These objectives are best achieved with the use of state space system models. Hence, our system is structured as a state space time domain model.

With an objective of developing the system model in the state space structure, the physical models of the previous chapter are designed in a fashion that are readily convertible to such a structure. Hence, the physical models of Chapter 2 are formulated in a way to use state variables explicitly. Table 6 lists the state variables used in the system model.

3.2 Differential Algebraic Equations

A linear time invariant (LTI) state space model is of the form $dx/dt = Ax(t) + Bu(t)$, $y(t) = Cx(t) + Du(t)$, where t is time, $x(t)$ is a vector of state variables, $u(t)$ is excitation, and $y(t)$ is the vector of responses. In such a formulation, the memory dynamics are incorporated in the state vector, and the output is a simple mapping of the state vector.

The auditory system model developed in this research uses a generalization of the LTI model, called differential algebraic equations (DAE). This model is of the form $M(t, x(t), u(t))dx/dt = f(t, x(t), u(t))$ and $y(t) = g(t, x(t), u(t))$, where

Table 6: State variables

Notation	Description
x_d	Displacement of diaphragm
v_d	Velocity of diaphragm
P_d	Pressure at diaphragm
x_m	Displacement of malleus
v_m	Velocity of malleus
$_i f_{li}$	Force by incus on i-m lever at the level of incus
x_s	Displacement of stapes
v_s	Velocity of stapes
P_{fl}	Differential pressure of fluid section, $P_{sv} - P_{st}$
x_{rl}	Displacement reticular lamina section
v_{rl}	Velocity of reticular lamina section
Q_{ohc}	Charge accumulation on the OHC membrane
v_{ohc}	Time derivative of contraction of OHC of section
V_{ohc}	Voltage across OHC membrane of section

M is the mass matrix that may be singular to allow in part purely algebraic constraints between state variables.

Examination of the left hand sides of the physical model equations of Chapter 2 reveal that they represent the mass matrix, M, and the right hand sides are the mappings, $f()$. The system resulting from the physical model is of the form $M dx/dt = f(x(t), u(t))$ with constant mass matrix, and $f(x(t), u(t)) = Ax(t) + Bu(t)$ for the linear case.

As the physical equations governing the cochlea have both time and space dependence and the differential algebraic equations have only time dependence, space discretization is required. Space discretization allows utilization of the differential - algebraic structure, whereas treatment of the physical models as a distributed system would not make it amenable to canonical partial differential equations with numerical solutions.

Discretization is conducted by expanding state variables that are space dependent into state variables for each section. Thus, for example, displacement of the reticular lamina, $x_{rl}(t)$, and time derivative of contraction of OHC, $v_{ohc}(t)$ are expanded into $x_{rl}^i(t)$ and $v_{ohc}^i(t)$ as state variables.

Just as space is discretized, time may also be discretized to yield algebraic system of equations instead of differential algebraic system of equations [22]. In this research, time is not discretized because robust solvers exist for differential algebraic equations. These solvers integrate the system of equations from the initial time to the final time with initial conditions for the state variables, and are expected to yield more accurate results than the discretized algebraic equations, as seen in the results chapter.

Space Discretization To determine the space discretization interval, empirical observation on animals that relates characteristic frequency to distance

from base of cochlea exponentially is used. In order to obtain a characteristic frequency resolution of 0.0021 octaves, a discretization of 700 sections over a length of 3.5 cm, with an interval length of 50 micro m (0.005 cm) is needed. This interval length is of the same scale as a hair cell length of 10 micro meters [9]. The equations below derive the desired space discretization interval.

$$\frac{CF^i}{CF^{i+1}} = \exp \frac{-(x^i - x^{i+1})}{len}$$

Since, $\Delta x = \frac{len}{numSec}$, then,

$$\frac{CF^i}{CF^{i+1}} = \exp \frac{1}{numSec}$$

And therefore, the frequency resolution $CF^i - CF^{i+1}$ is,

$$CF^i - \frac{CF^i}{\exp \frac{1}{numSec}}$$

As the calculation above shows, the discretization of 700 intervals results in a resolution of 28 Hz at characteristic frequency of 20 kHz at the base and a resolution of 0.014 Hz at characteristic frequency of 10 Hz at the apex.

3.3   Excitation and Response

The external stimulus applied in experiments on living human beings is the force at the diaphragm, $F_d(t)$. Stimuli at other locations are possible using intrusive surgery or through experiments on dead animals and cadavers. In this research stimulus at the diaphragm is considered as the sole excitation.

As the focus of this research is on the cochlea, the responses are variables that may be inputs or outputs of the cochlea. Thus, the responses are displacement of the stapes, x_s, and displacement of a reticular lamina section, x_{rl}^i. Other variables such as Q_{ohc}^i may also be considered as responses, but displacement of a reticular lamina is the main variable characterizing the cochlea.

The excitation and response define the boundary of the system, S, under consideration. Hence, the systems under consideration are S^{base}, cochlea starting at the stapes and ending at the base; S^{mid}, cochlea starting at stapes and ending at the middle section; S^{apex}, cochlea starting at stapes and ending at the apex of the cochlea; and S^i, cochlea starting at stapes and ending at the ith section of the cochlea. The input to these systems are x_s and the outputs are x_{rl}^{base}, x_{rl}^{mid}, x_{rl}^{apex}, and x_{rl}^i.

The force at the diaphragm in the external canal is in general not equal to the force at the ear drum, and the force at the ear drum is not the same as the force on the stapes. However, if the outer and middle ear systems are thought to contribute only insignificantly to tuning or delay, the displacement of the diaphragm or the ear drum may be approximated as the displacement of the stapes. This research work does not make this simplifying assumption as the system from the diaphragm to the stapes does not have unit transduction.

32

The major types of excitation are impulse, pure tone, white noise, and click. The impulse has a flat frequency spectrum allowing study of response at all frequencies, pure tone has an impulse frequency spectrum allowing study of only a single frequency, white noise has a flat spectrum, and click is a random signal used traditionally in physiological experiments covering a band of frequencies.

The ordinary differential equation solver used for numerical implementation not only integrates forward in time, but also backtracks in time with irregular intervals, thereby ruling out the use of random stimuli such as clicks and colored noise as discrete random signals.

As we are simulating a continuous time system using discrete simulation, an impulse in continuous time would correspond to a box car in discrete simulation. The boxcar corresponding to a unit continuous time impulse has a width equal to the time interval (for uniformly sampled) and a height that is the reciprocal of the time interval.

If the time sampling interval internal to the ode solver is constant, an impulse is characterized as having a value of $\frac{1}{6.25e-6}$ at only one particular time sample and zero otherwise, for a sampling interval of $6.25e - 6$. In our case, the ode solver has adaptive time intervals internally. Hence the impulse is characterized as a box car with an amplitude of $\frac{1}{6.25e-6}$ and a width of 6.25e-6. The start of the impulse is placed at 0.005 sec to visualize the changes from rest condition.

For tones, we use a multitude of tone stimuli have a range of 100 Hz to 20 kHz, with increments of 1 kHz. This allows covering of the spectrum of interest with suitable frequency resolution.

3.4 Subsystem Stabilization

Although the system of differential algebraic equations based on physical models may be solved in its current form, it may result in unbounded response to bounded excitation because of either subsystem instability or system instability. This section considers the issue of subsystem stability, focusing on each of the physical models of Chapter 2, and the next section addresses system stability.

This section uses s-domain analysis to determine stability of a subsystem. A subsystem is any of the physical models of Chapter 2. Consider a hypothetical linear subsystem, $d^2y/dt^2 + ady/dt + by(t) = pd^2u/dt^2 + qdu/dt + ru(t)$. If $u(t)$ is input and $y(t)$ is output, the subsystem is unstable if the roots of $s^2 + as + b$ are in the right half plane. If $y(t)$ is input and $u(t)$ is output, then the subsystem is unstable if the roots of $ps^2 + qs + r$ are in the right half plane. As may be noted in the physical model equations, a variable may be both an input and an output. And hence, both sides of the equation need to be analyzed. The subsystem is marginally unstable if the roots are on the imaginary axis. Care should also be taken if there is pole zero cancellation by omitting the common terms. If a linear equation has more than one input, the rules of superposition may be used to determine subsystem stability.

The remaining paragraphs of this section, analyze each subsystem of the physical model to determine instability, and then transform the equation to stabilize without changing the underlying physical model.

In the passive implementation of the model, it is assumed that the motion of the cochlear partition does not alter the receptor current through the hair bundle. Therefore, in the passive implementation, the following variables are negligible: $i_r, V_{ohc}, Q_{ohc}, x_{ohc}, v_{ohc}$, and hence the contraction force by the OHC on the RL and BM is negligible.

In investigating the stability of subsystems, we focus on those that are functional only in the active implementation - equations (29, 33, 30, 31). In the linear active implementation, all subsystems behave linearly, and in the nonlinear active implementation all subsystems behave linearly, with the exception of the relationship between RL motion and receptor current.

In equation 29, we find a pole-zero cancellation, which could lead to numerical errors causing instability.

$$sQ_{ohc} = sx_{ohc}/T_{ohc},\qquad(39)$$

Investigating V_{ohc} as a function of x_{ohc} in equation 31, we find the zero to be at s = 0 making the subsystem marginally unstable.

We also find that one of the poles of x_{ohc} as a function of V_{ohc} in equation 30 is when s = 0, making the subsystem marginally unstable - the other pole is when s is negative.

The pole-zero cancelation and the marginally stable relationships above were resolved by de-identifying x_{ohc} and instead only dealing with v_{ohc} as a state variable. However, the behavior of the active system did not change and was still unsteady.

We find that the s at which poles of x_{rl} as a function of x_{ohc} in equation 33 occur depend on the value of parameters.

$$s = \frac{1}{2m_{bm}}(-c_{bm|ohc} \pm \sqrt{c_{bm|ohc}^2 - 4k_{bm|ohc}m_{bm}})\qquad(40)$$

For the parameter values used (both in [22] and [23]) this relationship is stable. This is also the case with the poles of x_{rl} as a function of Q_{ohc} in equation 33, and the poles of x_{rl} as a function of Q_{ohc} in equation 32.

In equation, 32, we find that the zeros of x_{rl} in terms of x_{ohc} are at s = 0 and at $s = +c_{bm|ohc}/m_{bm}$. The positive root of s, suggests that the subsystem is unstable. Rewriting, equation 32 as equation 33, resolves the instability ($s > 0$) and the de-identification of x_{ohc} resolves the marginal instability.

This alteration makes the nonlinear active system appear stable. In the linear active implementation when using the parameters in table 5, the behavior of x_{rl} of the apical sections appear to be stable. However, the basal sections are unstable - though the blowing up of x_{rl} is 5 orders of magnitude less than when using 32.

3.5   System Stability

Subsystem stability does not necessarily imply system stability because of multiple loops characterizing the system. However, unlike the case of subsystem

instability which should be resolved through manipulations that do not effect the underlying physical phenomenon, system stability is a given and the objective is to determine whether the system is unstable rather than trying to stabilize it.

The systems of interest are S^{base}, S^{mid}, S^{apex}, and S^i. Ideally , stability of each of these systems should be determined, which is impractical. To overcome this problem, we consider the entire system, S, with input being the excitation at the diaphragm and output being the state vector encompassing all variables of interest in all sections. If the system, S, is stable, it has bounded state vector values for bounded excitation, thereby ensuring that all responses are bounded.

Stability of the system is determined as follows for linear time invariant systems - both passive and active. Consider the differential algebraic equation,

$$M \frac{dx}{dt} = Ax(t) + Bu(t)$$

Taking the Laplace tranform yields,

$$X(s) = (sM - A)^{-1} Bu(t)$$

The system is unstable if the eigenvalues of (sM - A) are in the right half plane and marginally stable if the eigenvalues are on the imaginary axis [49, 5, 16, 51]. Thus determining stability is the same problem as solving the generalized eigenvalue problem. The QZ algorithm is used to calculate the generalized eigenvalues.

3.6 Spectrum, System, and Frequency Response

As all variables are deterministic (non-random), the spectrum of a variable is computed by taking its Fast Fourier Transform (FFT). We compute the spectra of a state variable using an FFT size of 2^{17}. The frequency resolution of the spectra is thus 0.6 Hz $= \frac{1}{2^{17}} * 80$ kHz. This is sufficient resolution to handle all frequencies of interest, as the smallest characteristic frequency (CF) is expected to be 10 Hz.

As a linear time invariant system is fully characterized by its frequency response, we calculate the frequency response of the cochlea and the stapes, The frequency response of the cochlea is computed as the ratio of the spectrum of x^i_{rl} to the spectrum of x_s. The frequency response of the stapes is calculated as the ratio of the spectrum of x_s to the spectrum of x_i, the displacement of the incus.

The above process is restricted to calculation of the frequency response only at frequencies where the input spectrum has non-zero value. Hence, the advantage of using impulse as excitation. It should be noted however that an impulse excitation may produce zero values at some frequencies of the input spectrum, thereby allowing computation of frequency response of a system only at a subset of frequencies.

For the pure sinusoidal inputs - not studying the ramped up one, the system response spectrum cannot be studied due to numerical errors that arise due to

division by zero input for nonresonant frequencies. Instead, for any tonal input, the output is considered, as the middle ear system is not expected to hinder the detection of resonant frequencies, except if the sinusoid used is at the low resonant frequency of the middle ear.

The frequency response of a linear system with tone excitation may only be calculated at the frequency of the excitation because the excitation has no other frequency content. Hence the frequency response of a linear system may be calculated by exciting the system with a multitude of tones and determining the ratio of output and input spectrum at that frequency (or alternatively amplitude amplification and phase shift of the response) for each of the excitations. We use this approach for validation only, as the method using impulse excitation is more practical. Otherwise, we would have to stimulate with several tones of differing frequencies.

In the linear simulation of the cochlea, or low level stimuli using nonlinear simulation (which behaves linearly up to 40 dB), the resonant frequencies and the group delays derived from Fourier transforms using a broad band stimulus are expected to match those derived using tones, based on physiological experiments.

For nonlinear systems, the ratio of output and input spectra may be calculated for a specific input. However, this ratio is not the frequency response, as an input with a particular frequency would not yield an output of the same frequency with amplification and a phase shift. Also, superposition of input would not yield superposition of output. The ratio thus does not characterize the system completely and response to an arbitrary input cannot be computed from the ratio for a particular input.

In the case that the excitation level is low, the system is only mildly nonlinear. Thus we calculate the spectral ratio treating the system as if it were linear, making the ratio equivalent to the frequency response. This is validated by confirming that a tone excitation results in a response that is a tone with the same frequency as the excitation, and the frequency response computed from the multitude of tones is approximately the same as that calculated with impulse excitation. The threshold of excitation amplitude at which this is untrue is determined.

3.7   Frequency Domain Characteristics

This section presents response and system characteristics in the frequency domain. Responses are characterized by the spectra of x_s, x_{rl}^i. Systems are characterized by the frequency response of S^{base}, S^{mid}, S^{apex}, and S^i representing cochlea starting at the stapes and ending at a section.

3.7.1   Response Characteristics

Spectral magnitude of x_s, x_{rl}^{base}, x_{rl}^{middle}, and x_{rl}^{apex} are plotted to determine general frequency domain characteristics of the response to impulse excitation. The peak frequencies and bandwidths of the spectra of x_s, and x_{rl}^i for all i are

used as parametric characteristics of the responses. The peak frequencies are computed by identifying the local maxima of the spectrum magnitude and the bandwidth are calculated as in equations 43 and 44.

These spectral characteristics are calculated for the passive linear, active linear, and active nonlinear systems with impulse as an excitation. In addition, they are calculated for tones as excitation for purposes of validation. This is especially useful in determining the threshold of amplitude of excitation for the nonlinear systems to be approximated as linear. The derived spectral characteristics are discussed in the context of existing literature.

3.7.2 System Characteristics

The frequency responses of the stapes and cochlea are calculated from the ratios of their output to input spectra with impulse as an excitation. These frequency responses are examined visually at the cochlea base, middle, and apex for general characteristics

The parameters characterizing the frequency response are resonant frequencies, bandwidth, ERB, QERB, and group delay (N_{rl}). These are computed as follows for all space indexes of the cochlea and the stapes. TF is the spectral ratio of output and input representing the transfer function and ϕ is the unwrapped phase.

$$CF^i = \arg max(|TF^i|) \tag{41}$$

$$N_{rl} = -\frac{1}{f}\frac{d\phi}{df} \tag{42}$$

The ERB is calculated using two separate methods to be able to compare results with studies that use either measure. The more traditional method of measuring ERB is as in equation 43 [45], but one of the studies uses a second measure of ERB as in 44 [22].

$$ERB = \frac{1}{TF_{max}^2}\int |TF|^2\,\mathrm{d}f \tag{43}$$

$$ERB = \frac{1}{TF_{max}}\int |TF|\,\mathrm{d}f \tag{44}$$

We study the x_s (input), the x_{rl} (output) for various sections, and the system TF for various sections - where applicable, in the time domain and the frequency domain for the different stimuli. We use these measures to extract the characteristic frequencies (CF) vs space maps as well as the ERB and sharpness of tuning, QERB. We also study contour plots given tonal stimuli.

37

4 Numerical Implementation

This chapter presents aspects related to implementation of the system model. Section 4.1 examines the choice of equation solvers for our initial value problem. Section 4.2 presents the tolerances used in the iterative solvers. Section 4.3 derives analytically the time duration of simulation to ensure proper measurement. Section 4.4. computes the time sampling interval needed to simulate the continuous system using a discrete solver.

4.1 Ordinary Differential Equation Solver

As the system of equations governing the physical model is a differential algebraic equation (ie with a singular mass matrix), rather than a pure differential equation, only methods that allow for singular mass matrices may be used. In the case of Matlab, these are ode23t and ode15s [39, 40]. These routines solve the linear algebraic equation for the state variables at different times using $Mx' = f$, where x is the vector of state variables, and M is the constant mass matrix of x coefficients.

ode23t is an implementation of the trapezoidal rule using a "free" interpolant. It can be used only if the problem is moderately stiff and a solution is needed without numerical damping. ode15s is a variable order solver based on numerical differentiation formulas (NDFs). It is a multistep solver, that is appropriate when the problem is stiff. As our system is stiff for active system and moderately stiff for passive system (as discovered during implementation), we use ode15s . If we had used ode23t, the tolerance would have had to be increased substantially for the active system.

4.2 Tolerance

For the passive implementation, the absolute error tolerance is set to 1e-6 and the relative error tolerance is set to 1e-3. For the stiffer (active) implementation, the absolute error tolerance is increased to 1e-5 and the relative error tolerance is increased to 0.2 due to limitations on the internal step size.

4.3 Time Span

The differential algebraic equations are integrated using the ode solver ode15s from time = 0 with initial rest conditions till time 0.005 sec to time = 70 msec. Time of excitation made non-zero to visualize the changes from rest condition.

The span is chosen by considering a second order system. The denominator of the transfer function of a second order system with natural frequency ω_0 and damping factor ζ is as follows [4]

$$1s^2 + 2\zeta\omega_0 s + \omega_0^2 \tag{45}$$

As the 3dB quality factor, Q_{3dB} is ω_0/BW_{3dB}, and $\zeta = 1/2Q_{3dB}$. The settling time for a second order system is $-\ln(tolerance)/\zeta\omega_0$, where the tolerance

is the error band within which the response to a step excitation remains after settling time. Hence settling time is $-2\ln(tolerance)/BW_{3dB}$

The smallest ERB of the auditory system is 50. Approximating this as a value for BW_{3dB} and assuming that tolerance is 15%, the settling time is then $0.07s$.

The simulation run time is 70 msec, large enough for all input frequencies to reach steady state, and to travel from the ear canal to the apex of the cochlea, and back again (to detect possible reflections) taking into account the variable acoustic wave speed within the cochlea. The stimuli are allowed to run for 70 msec for the responses to reach the very apex of the cochlea, and for all frequencies within the humans hearing range to reach steady state.

4.4   Time Sampling Interval

In order to determine the time sampling interval for integration, we utilize the fact that sampling rate should be larger than twice the highest non-zero frequency to avoid aliasing (Nyquist criterion). The highest characteristic frequency is 20 kHz, and hence we can assume that the spectrum is negligible for frequencies above 40 kHz; the Nyquist frequency is therefore 80 kHz. This implies that the sampling interval is larger than $1.25e - 5 = 1/(2 * 40kHz)$. In many cases we take fast Fourier transform (FFT) of a signal, which has a length that is power of two for efficient implementation. Our sampling rate can be between 1.25e-5 and $7.6e - 6 = \frac{1}{2^{17}}$ to utilize the same size FFT. We thus choose a sampling interval of 6.25e-6 sec.

The sampling interval is utilized as the maximum allowed step size in the ode solver. The actual internal step size varies with time as it adapts based on the rate of change of the solution. The values of excitation and response are resampled at uniformly spaced time sampling intervals 6.25e-6 sec apart.

The solution of the ode solver sampled at intervals of 6.25e-6 seconds allows for detecting frequencies up to 80 kHz to guard against aliasing problems; since the highest CF in humans in 20 kHz, and the filters are narrowly tuned, it is expected that the frequency response of the most basal sections would have decayed by 4*the highest CF (80 kHz). This is expected to reduce the uplifting of the system frequency response at higher frequencies, and its validity is discussed further in section 5.

5 Results

This chapter presents results of numerical implementation, and discusses their validity against previous studies. We present the waveform of the response in the cochlea represented in the time domain and it's progression through space. We then study the tuning characteristics of the middle ear. We investigate individual system transfer function characteristics, as well as characteristics (such as characteristic frequency CF, equivalent rectangular bandwidth ERB, sharpness of tuning Q_{ERB}) as a function of space and CF. As the parameters in Table 4 are in cgs units, so are the plots in this chapter.

5.1 Traveling Wave
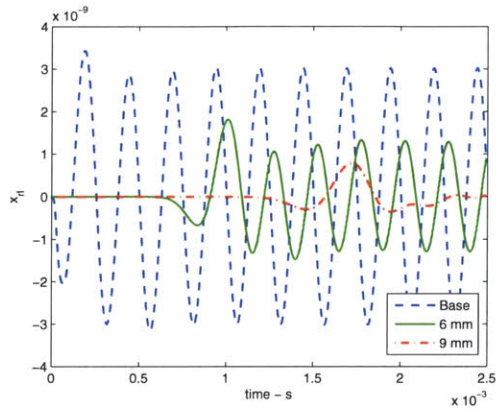
Figure 6: Traveling wave x_{rl} in response to 4 kHz tone
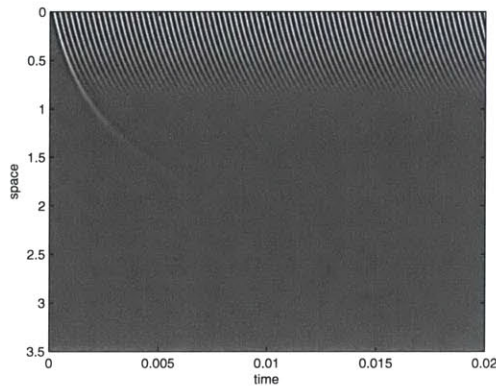
Figure 7: Response of $x_{rl}^i(t)$ to 4kHz

40

Figure 6 shows an example of the simulated traveling wave produced in the cochlea in response to a 4 kHz sinusoidal stimulus using the passive implementation. As expected, the time delay for the wave to reach more apical sections is greater than the base. Also, the response to the 4 kHz stimulus decays substantially after the space section where the CF is 4 kHz (0.35 cm from the base as seen in figure 12).

The traveling wave progression can also be seen as a function of space and time (in response to a 4 kHz sinusoidal stimulus) in figure 7. Interestingly, no reflection is seen at the helicotrema after running the simulation for 70 msec, despite the inductive boundary condition at the apex (equation 18).

5.2   Tuning Characteristics of Middle Ear

Figure 8 shows the spectrum of x_s in response to an impulse. The spectrum of x_s is equivalent to the transfer function of the middle ear system, since an impulse stimulus has a spectrum of 1 for all frequencies. This shows that there is a single resonant frequency of the outer and middle ear of 765 Hz, which is close to the resonant frequency of 900 Hz experimentally measured from previous studies [34].

Two methods are used to calculate the ERB as they are two measures used in the literature; using equation 44 gives an ERB estimate of 2 kHz, and using equation 43 gives an estimate of 1.36 kHz.
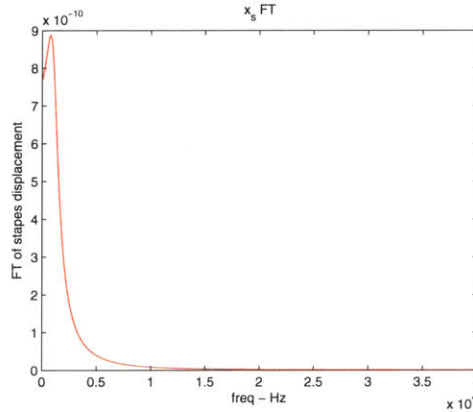

Figure 8: Stapes displacement spectrum

5.3   Spectrum of Reticular Lamina Displacement

Figures 9 show the spectra of the x_{rl} at various points along the cochlea in response to an impulse stimulus. The response of the middle section shows that frequencies above 2 kHz are insignificant. We would expect the magnitude of the response at frequencies above 2 kHz to be greater for the middle than the

41

apex. However, figure 10 shows that the magnitude of response for frequencies above 2 kHz of the apex is greater than that of the middle. This may be a result of the boundary condition at the apex, and is explored further in the following sections.
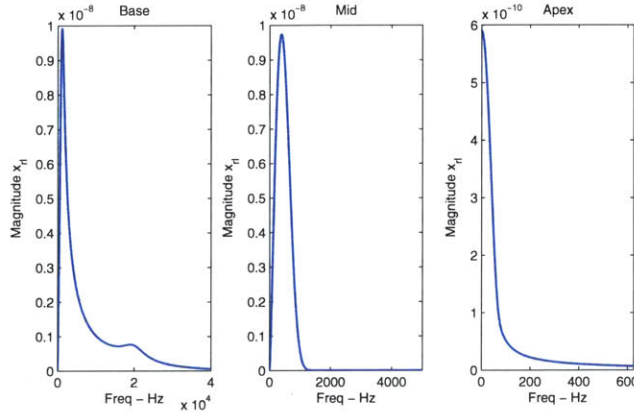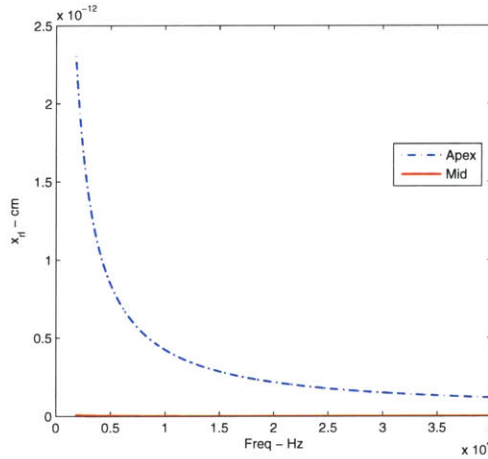

Figure 9: Spectra x_{rl}

Figure 10: Spectra x_{rl} Mid, Apex about 2 kHz

5.4   General System Characteristics

The magnitude and phase of the frequency response of systems S^i, with input x_s and outputs x_{rl}^i, is studied. The results shown in Figure 11 are the passive

system's response to an impulse stimulus, and show single resonances for each of the sections.

For the most basal and the most apical sections, the spectrum of x_s continues to decay at higher frequencies, but the spectra of x_{rl} begin to flatten out at higher frequencies. This results in the uplifting of the higher frequencies in the transfer functions of the basal-most sections - up to 0.17 cm, and apical-most sections - down to 2.09. If unaccounted for, this uplifting would create an error in measures of bandwidth such as ERB, but not BW3dB. We therefore only calculate the ERB for system FTs of sections 0.17-2.09 cm along the length of the cochlea. We confirmed that the uplifting is not due to numerical errors.
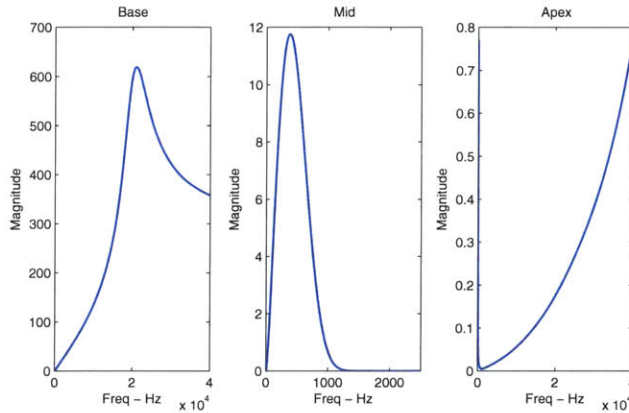

Figure 11: System TF

5.5   Cochlear Map

We calculate the resonant frequencies of each cochlear section using an impulse stimulus, and validate a few CF-space relationships using tonal excitations. Figure 12 shows a logarithmic relationship between CF and space; with CF decreasing from base (with a maximum CF of 20 kHz) to apex (minimum CF of 10 Hz). These observations are consistent with the results of previous studies [9, 22].

Because of uplifting higher frequencies in the transfer functions of the most basal sections, it is possible that the higher CFs (of the basal sections) extracted from the system transfer functions are slightly higher than the true CFs for those locations. However, comparing the output FTs (figure 9) with the transfer functions show that this overestimation is very small relative to the CFs of the basal sections.

The CF cannot be estimated directly for sections more apical than 2.83 cm, due to the great amount of uplifting of high frequencies. We therefore cap the maximum frequency detectable for the CF to 2.5 kHz of the most apical regions to get figure 12.
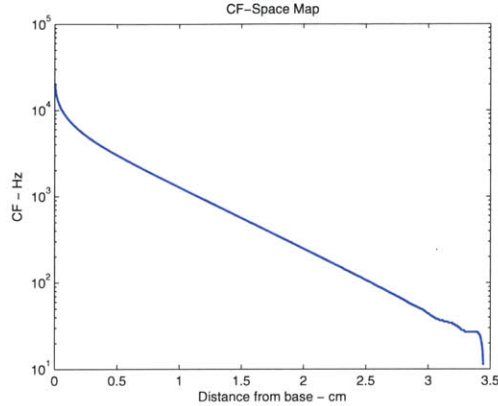
43

Figure 12: CF-Space map

5.6   System TF Variation Along the Cochlea

We look at the magnitude and phase of the system transfer functions (TF) as a function of space for particular frequencies in the impulse stimulus. Figures 13 and 14 show this for the passive implementation and in particular for the frequencies 240 Hz, 1.2 kHz, and 3.66 kHz. The magnitude of the system transfer function to any particular frequency increases slightly with space until it reaches the space section with that frequency as a resonant frequency (where it is maximally amplified), then quickly decays, as would be expected from the cochlea which allows for transmission of frequencies until they reach their sections of maximal amplification. Interestingly, however, the frequency response then increases and has minor peaks for two of the apical-most sections. This two minor peak behavior, the small time step size chosen, and the fact that the uplifting occurs for all frequencies after decaying at their place of resonance suggests that the uplifting seen in the system transfer function of Figure 11 is probably not due to aliasing problems, but rather due to inherent model behavior. As the transfer function magnitude is bolted to a particular nonzero value for all frequencies in figure 13, this suggests that the boundary condition at the apex (equation 18) is incorrect. The drastic change in the CF-space relationship at the apical sections in figure 12 also supports this conclusion.

For a delayed signal $x(t - t_0)$, the Laplace transform is $e^{-st_0} X(s)$ where X(s) is the Laplace transform of x(t). Therefore the phase delay in figure 14 is calculated as $\frac{\phi}{2\pi f}$. The phase delay increases with distance as expected. The figure shows an almost linear phase delay that is independent of frequency until the place of resonance where the magnitude of the system TF is nonzero, as would be expected in the cochlea, because a signal of frequency less than or equal to the resonant frequency would be expected to reach that CF point in the cochlea without deformation and purely with time delay.
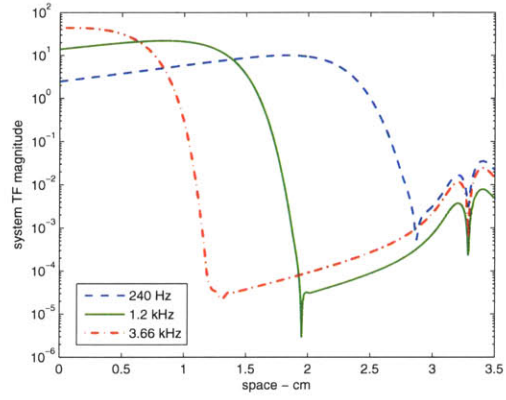
44

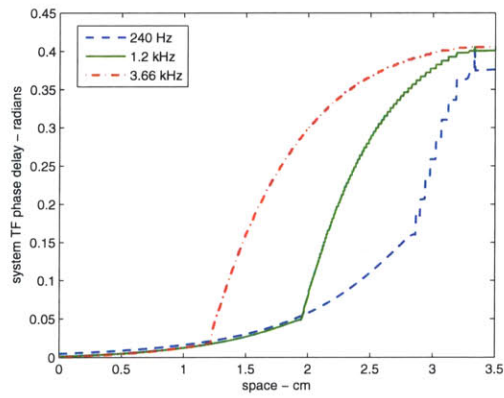Figure 13: System FT magnitude as a function of space

Figure 14: Delay as a function of space

45

5.7 Group Delay

The nondimensionalized group delay $N_{rl} = -\frac{1}{f}\frac{d\phi}{df}$ is plotted for CFs given an impulse stimulus to the passive implementation (the relationship using the active implementation is similar). The relationship between N_{rl} and CF is shown to be logarithmic (figure 15) as consistent with previous studies that approximate the group delay at the CF (of active cochlea) from the group delay of SFOAEs. However, N_{rl} appears to decrease with CF, which is the opposite of what is expected based on these studies [43].
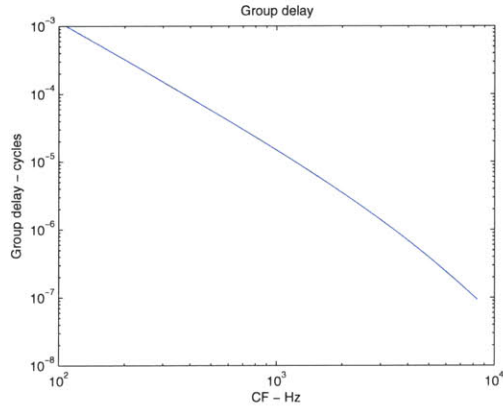

Figure 15: Group Delay - CF

5.8 Bandwidth and Sharpness of Tuning

Figures 16 and 17 show that ERB and Q_{ERB} as measures of bandwidth and sharpness of tuning of the passive system using the ERB in equation 43. Figures 18 and 19 show that ERB and Q_{ERB} of the passive system using the ERB in equation 44. Both calculations show that $ERB \approx CF$. Therefore ERB decreases from base to apex, as is consistent with the results of previous studies [22].

Simultaneous psychoacoustic studies (as described in Chapter 1) suggest that the sharpness of tuning, Q_{ERB}, increases exponentially with CF until around 1kHz, after which it starts plateauing [22, 26, 43]. Nonsimultaneous psychoacoustic studies on humans, as well as experimental studies on animals, suggest that the Q_{ERB} continues to increase exponentially with frequency [26, 43]. Both calculations also show a plateauing of Q_{ERB} around 1 kHz, as is observed with nonsimultaneous studies. However, both calculations show that the Q_{ERB} increases after 1 kHz, consistent with nonsimultaneous studies - though the relationship between Q_{ERB} and CF is nonexponential. For CF below 1 kHz, Q_{ERB} increases with CF exponential with CF when using equation 44 which is consistent with both types of psychophysical studies on humans and experi-

mental studies on animals [26]. Using equation 44, on the other hand, gives the opposite result. We do not expect the ERB and Q_{ERB} results for the passive implementation to correspond directly to that of such psychophysical studies which are reflective of the nonlinear active cochlea. We do not discuss the ERB and Q_{ERB} of the active implementation, due to the greater dependence of stability and ERB results on the number of sections for the parameters chosen. Further validation of the active version is required.
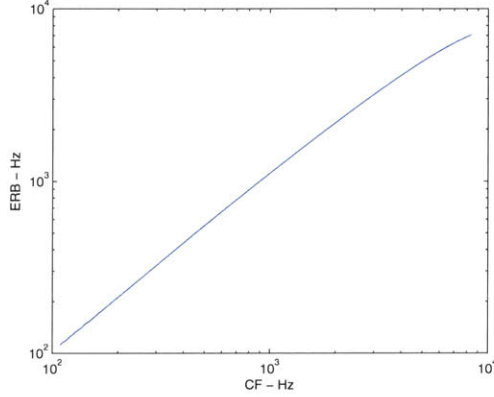

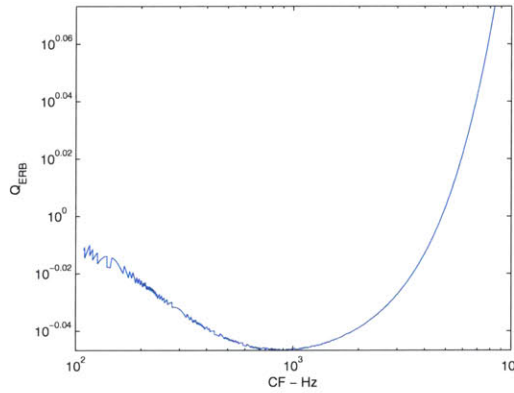Figure 16: ERB using equation 43

Figure 17: Q_{ERB} using equation 43

Studies that derive relationships between $N_{rl}(f = CF)$ and Q_{ERB} from filter theory models suggest that $N_{rl}(f = CF) = kQ_{ERB}$, where k is independent of CF [41, 43]. Our results are inconsistent with these studies.
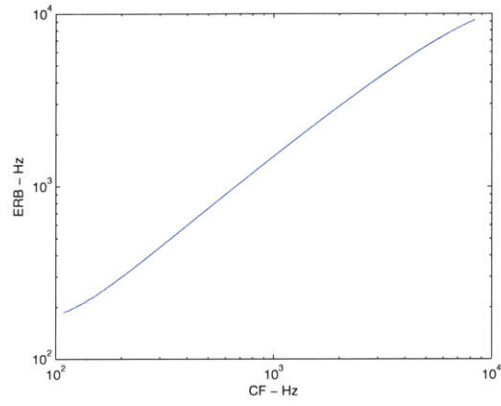
47

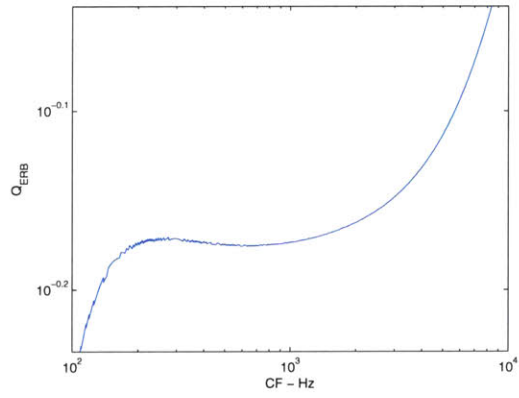Figure 18: ERB using equation 44

Figure 19: Q_{ERB} using equation 44

48

6   Conclusion

Summary This study developed a modeling approach and an implementation toolset to simulate reticular lamina displacement in response to excitation at the ear canal and to characterize the cochlear system in the frequency domain.

Physical models were developed for the outer, middle, and inner ears based on mechanical, acoustic and electrical lumped and distributed laws. These physical models were formulated as differential algebraic state space system of equations and methods were presented to determine the stability of the system.

The auditory system was simulated using an impulse and solved using an ordinary differential equation solver. Frequency domain characteristics of basilar membrane displacement and partitions of the cochlea were determined. These included generation of the cochlear map, group delay, ERB, and QERB.

Recommendations The methodology followed in this research demonstrated the benefits of utilizing careful physical modeling alongside differential algebraic state space system. Such an approach allows for control over accuracy of results, time, frequency, and space resolution. This comes at the expense of computational efficiency, however, with the implementation requiring 2.5 hours of run time and a memory use of 5 GB for the parameters and tolerances used and for analysis of all variables for 700 space sections. This necessitates use of a 64 bit operating system and 64 bit Matlab.

Conclusions Characteristics obtained in this paper have been compared with findings from existing studies, whether experimental, theoretical, or computational. These include conclusions regarding the nature of the traveling wave, tuning characteristics of the middle ear, cochlear map, group delay, ERB, and QERB. The main point of departure has been behavior at the apex, which did not yield expected results.

Future Directions There are two areas of improvement that may be made. First, physical laws at the apical boundary need to be revisited as it seems to enforce incorrect boundary conditions. Second, the equations and parameters should be revised to ensure system stability beyond a certain number of sections.

The toolset may be tested by comparing its results to Zweig's transmission line model for passive system for which an analytical solution is derived [53]. Other suggestions for future research include utilization of partial differential equations rather than discretizations of space, and staged development of refined physical models. Also, future simulation of the cochlea alone, without the outer and middle ear would allow for further insights into system behavior.

References

[1] Bear M., Connors B., Paradiso M., *Neuroscience: Exploring the Brain*. Lippincott Williams and Wilkins. 3rd edition, 2006.

[2] Beurg M., Fettiplace R., Nam J-H., Ricci A.J., *Localization of inner hair cell mechanotransduction channels using high-speed calcium imaging*. Nat Neurosci, 2009, 12:553-558

[3] Braida L., *MIT 6.551 course notes: Perception*. MIT, Fall 2010.

[4] Dorf R., Bishop R., *Modern Control Systems*. Prentice Hall, 12 edition, 2010.

[5] Fairman F., *Linear Control Theory: The State Space Approach*. John Wiley and Sons, July 7, 1998.

[6] Feilding C., *College of Santa Fe - Auditory Theory Lecture Notes 6: Hearing I*. College of Santa Fe.

[7] Fettiplace R., Heckney C., *The sensory and motor roles of the auditory hair cells*. Nature Reviews Neuroscience, 2006.

[8] Fuchs P., *Oxford Handbook of Auditory Science The Ear - Chapter 3: External and middle ear function*. Oxford university press, Feb 2010.

[9] Geisler D., *From Sound to Synapse: Physiology of the Mammalian Ear*. Oxford University Press, 1998.

[10] Ghaffari R., Aranyosi A.J., Freeman D.M., *Longitudinally propagating traveling waves of the mammalian tectorial membrane*. Proc Natl Acad Sci USA, 2007;104:16510.

[11] Goodyear R.J., Marcotti W., Kros C.J., Richardson G.P., *Development and properties of stereociliary link types in hair cells of the mouse cochlea*. J. Comp. Neuro., 2005, 485, 75-85.

[12] Guinan J., *MIT HST 723. Neural Coding and Perception of Sound course notes: Functional cochlear mechanics*. MIT, Spring 2011.

[13] Howard J., Hudspeth A.J., *Compliance of hair bundle associated with gating of mechanoelectrical transduction channels in the bullfrog's saccular hair cell*. Neuron, 1988, 1:189-199.

[14] Hudspeth, A.J., *How the ear's works work*. Nature, 1989, 341, 397-404.

[15] Kachar B., Parakkal M., Kurc M., Zhao Y., Gillespie P.G., *High-resolution structure of hair-cell tip links*. Proc. Natl. Acad. Sci. USA, 2000, 97, 13336-13341.

[16] Kailath T, *Linear Systems*. Prentice-Hall, Inc., 1980.

[17] Karavitaki K.D., Mountain D.C., *Evidence for outer hair cell driven oscillatory fluid flow in the tunnel of corti*. Biophys J, 92, 3284-93. 2007.

[18] Liberman C., Maison S., Eatock R-A., *MIT HST.721 Lecture*. MIT, Fall 2010.

[19] Lim K., Park S., *A mechanical model of the gating spring mechanism of stereocilia*. Journal of Biomechanics, 2009, 42:2158-2164.

[20] Liu S., White R., *Orthotropic material properties of the gerbil basilar membrane*. J. Acoust. Soc. Am., 123 (4), 2008.

[21] Liu Y-W., Neely S., *Outer hair cell electromechanical properties in a nonlinear piezoelectric model*. J. Acoust. Soc. Am., 126(2), August 2009, 751-761.

[22] Liu Y-W., Neely S., *Distortion product emissions from a cochlear model with nonlinear mechanoelectrical transduction in outer hair cells*. J. Acoust. Soc. Am., 127(4), April 2010, 2420-2432.

[23] Liu Y-W., *Matlab script*. Jun, 28, 2010.

[24] Manley G., Fay R., Popper A., *Springer Handbook of Auditory Research: Active Processes and Otoacoustic Emissions - Chapter: Otoacoustic Emisions: Concepts and Origins, by Kemp*. Springfield, 2007.

[25] Miller C., *Structural implications of basilar membrane compliance measurements*. J. Acoustic Society Am., 77 (4), 1984.

[26] Moore B., *Psychophysical tuning curves measured in simultaneous and forward masking*. J. Acoust. Soc. Am., 63(2), Feb.1978 524-532.

[27] Naidu R., Mountain D., *Basilar Membrane Tension Calculations for the gerbil cochlear*. J. Acoustic Society Am., 121 (2), 2007.

[28] Nam J.H., Cotton J.R., Peterson E.H., Grant W., *Mechanical properties and consequences of stereocilia and extracellular links in vestibular hair bundles*. Biophys. J., 2006, 90, 2786-2795.

[29] Nam J.H., Cotton J.R., Peterson E.H., Grant W., *A virtual hair cell, I: addition of gating spring theory into a 3-D bundle mechanical model*. Biophys. J., 2007, 92, 1918-1928.

[30] Netter F., *Atlas of human anatomy*. Rittenhouse Book Distributors Inc., 2nd edition, January 15, 1997.

[31] Perez J., Alkhairy S., *MIT 20.310 Project: Cochlear mechanics with emphasis on basilar membrane mechanics*. MIT, Spring 2010.

[32] Portnoff M. R., *MIT thesis: A quasi-one-dimensional digital simulation for the time-varying vocal tract*. MIT, June 1973.

[33] Puria S. and Allen J., *A parametric study of cochlear input impedance.* J. Acoustic Society Am., 89(1), January 1991, 287-309.

[34] Puria S. and Allen J., *Measurements of human middle ear forward and reverse acoustics: Implications for otoacoustic emissions.* J. Acoustic Society Am., 113 (5), May 2003, 2773-2789.

[35] Quatieri T, *Discrete-time speech signal processing: Principles and practice.* Prentice Hall, Nov 8, 2001.

[36] Rugerro M., Rich N., *Furosemide alters organ of corti mechanics: Evidence for feedback of outer hair cells upon the basilar membrane.* The Journal of Neuroscience, April 1991, 11(4): 1057-1067.

[37] Sandham J., *Implanted Devices.* June 2006, Retrieved May 2,2011, from http://www.ebme.co.uk/arts/implant.

[38] Santos-Sacchi J, *New tunes from Corti's organ: the outer hair cell boogie rules.* Current Opinions in Neurobiology, 2003,13:459-468.

[39] Shampine, L. F. and M. W. Reichelt, *The MATLAB ODE Suite.* SIAM Journal on Scientific Computing, Vol. 18, 1997, pp 1-22.

[40] Shampine, L. F. and M. W. Reichelt, *Solving Index-1 DAEs in MATLAB and Simulink.* SIAM Review, Vol. 41, 1999, pp 538-552.

[41] Shera C., Guinan J., Oxenham A., *Otoacoustic Estimation of Cochlear Tuning: Validation in the Chinchilla.* Journal of the Association for Research in Otolaryngology, 2010.

[42] Shera C., Guinan, J., *Stimulus-frequency-emission group delay: A test of coherent reflection filtering and a window on cochlear tuning.* J. Acoust. Soc. Am., 113 (5), May 2003.

[43] Shera C., Guinan J., Oxenham A., *Revised estimates of human cochlear tuning from otoacoustic and behavioral measurements.* PNAS, March 5,2002 vol.99 no.5.

[44] Shera C., Guinan J., *Evoked otoacoustic emissions arise by two fundamentally different mechanisms: A taxonomy for mammalian OAEs* J. Acoust. Soc. Am., 105 (2), Pt. 1, February 1999.

[45] Siebert W., *Circuits, Signals and Systems.* The MIT Press, September 13, 1985.

[46] Sollner, C., Rauch, G.-J., Siemens, J., Geisler, R., Schuster, S.C., the Tubingen 2000 Screen Consortium, Muller, U., Nicolson, T., *Mutation in cadherin 23 affect tip links in zebrafish sensory hair cells.* Nature, 2004, 428, 955-959.

[47] Sukharev S., Corey D. P., *Mechanosensitive channels: multiplicity of families and gating paradigms.* Science's stke, 2004, 219:1-24.

[48] Tsuprun, V., Santi, P., *Helical structure of hair cell stereocilia tip links in the chinchilla cochlea.* J. Assoc. Res. Otolaryngol., 2000, 1, 224-231.

[49] Van Dooren P., *The generalized eigenstructure problem in linear system theory.* IEEE Trans. Aut. Contr., Vol. AC-26, No 1, pp. 111-129, Feb. 1981.

[50] Warren R, *Auditory Perception: An Analysis and Synthesis.* Cambridge University Press, Third Edition, 2008.

[51] Zadeh L, Desoer C, *Linear System Theory: The State Space Approach.* Dover Publication, Jul 24, 2008.

[52] Zheng J, Weixing S, He D, Long K, Madison L, Dallos P, *Prestin is the Motor Protein of Cochlear Outer Cells.* Nature, vol.405, p.149-155, 11 May 2000.

[53] Zweig G., Lipes R., and Pierce J.R., *The Cochlear Compromise.* J. Acoust. Soc. Am., Vol. 59, No. 4, April 1976.